

1 **Mars *in situ* oxygen and propellant production by**
2 **non-equilibrium plasmas**

3 **P. Ogloblina^{1,2}, A. S. Morillo-Candas², A. F. Silva³, T. Silva¹, A.**
4 **Tejero-del-Caz⁴, L. L. Alves¹, O. Guaitella², and V. Guerra¹**

5 ¹Instituto de Plasmas e Fusão Nuclear, Instituto Superior Técnico, Universidade de Lisboa, Portugal
6 ²Laboratoire de Physique des Plasmas (UMR 7648), CNRS-Univ. Paris Sud-Sorbonne Universit-École

7 Polytechnique 91128 Palaiseau, France

8 ³Dutch Institute For Fundamental Energy Research (DIFFER), Eindhoven, The Netherlands

9 ⁴Departamento de Física, Universidad de Córdoba, Spain

10 **Key Points:**

- 11 • Vibrational temperatures and CO and CO₂ concentrations are measured for the
12 first time in plasmas created in realistic Martian conditions
13 • The temperature and pressure conditions on Mars favor vibrational non-equilibrium
14 • The minor constituents of the Martian atmosphere facilitate carbon dioxide dis-
15 sociation by electron impact

Corresponding author: Vasco Guerra, vguerra@tecnico.ulisboa.pt

Abstract

It has been recently advocated that Mars has excellent conditions for oxygen and fuel production directly from atmospheric CO₂ using non-equilibrium plasmas. The Martian conditions would be favorable for vibrational excitation and/or enhanced dissociation by electron impact, two important pathways for CO₂ plasma dissociation. Herein we confirm these theoretical predictions by measuring, for the first time, the vibrational temperatures of CO₂ and the CO and CO₂ concentrations in realistic Martian conditions. *In situ* Fourier transform infrared spectroscopy (FTIR) measurements are performed in experiments conducted in DC glow discharges operating at pressures $p = 1 - 5$ Torr, discharge currents $I = 10 - 50$ mA, initial gas temperatures of 220 K and 300 K, both in pure CO₂ and in the synthetic Martian atmosphere 96%CO₂-2%Ar-2%N₂. To analyse and interpret the experimental results, we develop a detailed self-consistent kinetic model for pure CO₂ plasmas, describing the coupled electron and heavy-particle kinetics. The simulation results are in very good agreement with the experimental data. It is shown that the low-temperature conditions may enhance the degree of vibrational non-equilibrium and that the Martian atmospheric composition has a positive effect on CO₂ decomposition. Accordingly, the present investigation confirms the potential of plasma technologies for in-situ resource utilization (ISRU) on Mars.

Plain Language Summary

In-situ resource utilization (ISRU) is a key concept in space exploration, corresponding to the harnessing of resources on the exploration site that would have to be brought from Earth otherwise. Mars is one of the main targets for future planetary missions. Its atmosphere is mostly formed by carbon dioxide (CO₂), a resource that can be used to produce locally the propellants for returning to Earth and oxygen for breathing in a future human outpost, by decomposing it into carbon monoxide and oxygen. Recently, it has been theoretically predicted that the red planet has nearly ideal conditions for CO₂ decomposition by non-thermal plasmas, due to the appropriate pressure and temperature and to the presence of argon and nitrogen as minor constituents. Here, we experimentally verify this conjecture, by measuring, for the first time, the conversion of CO₂ in a DC glow discharge operating at Martian conditions. The experiments are complemented with new simulations developed to describe and interpret the experimental results. We show that the low-temperature and pressure conditions may enhance the degree of vibrational non-equilibrium and that the Martian atmospheric composition has a positive effect on CO₂ decomposition, confirming the potential of plasma technologies for oxygen and fuel production on Mars.

1 Introduction

Mars exploration draws ever more attention nowadays, with new plans from space agencies and private companies announced frequently (NASA, 2020). Current missions to the surface of the red planet focus on robotic landers and rovers, but proposals for the first human missions and settlements will certainly follow soon. Future missions will require the ability to collect resources *in situ* and transform them into breathable air, water, propellants or food. Mars has resources that can be used for a sustainable settlement, such as carbon dioxide, which is the most abundant (95.9%) component of its atmosphere, with smaller percentages of Ar (1.9%), N₂ (2.6%) and other gases (Haberle, 2015). The local production of oxygen on Mars directly from atmospheric CO₂ may help solving some of these challenges, such as manufacturing fuels to get back to Earth, and creating a breathable environment for a future outpost.

The idea to try to use CO₂ as a raw material for *in situ resource utilization* (ISRU) on Mars for rocket propellant production dates back to the late 1970s, with the pioneering works of Ash and collaborators (Ash et al., 1978; Stancati et al., 1979). CO₂ can be

66 converted into carbon monoxide (CO) and oxygen (O₂) and used in a CO/O₂ propellant
 67 or, with some hydrogen brought from Earth or produced from Martian water, into
 68 oxygen and methane, the latter via the Sabatier process $\text{CO}_2 + 4\text{H}_2 \rightarrow \text{CH}_4 + 2\text{H}_2\text{O}$. Sev-
 69 eral authors have discussed the feasibility of using local resources for fuel or oxygen man-
 70 ufacturing, and the references given here are merely indicative. Landis and Linne (2001)
 71 proposed the construction of a reusable hopper vehicle that could self-refuel, making its
 72 fuel from a zirconia-electrolysis oxygen generation system. Boiron and Cantwell (2013)
 73 discuss the possibility of hybrid rocket propulsion systems, based on a combination of
 74 a liquid oxidizer and a solid fuel, where the oxidizer is acquired through decomposition
 75 of carbon dioxide on the surface of Mars. A review of the state-of-the-art on Mars ISRU
 76 was published in 2015 by Sanders et al. (2015). In the last few years, solid oxide elec-
 77 trolysis for fuel and oxygen production from the Martian atmosphere (Stancati et al.,
 78 1979) has caught a lot of attention, due to its choice for the thrilling Mars Oxygen ISRU
 79 Experiment (MOXIE) instrument on the Mars 2020 mission (Hartvigsen et al., 2015; Hecht
 80 et al., 2014; Hecht & Hoffman, 2016), a choice dictated by the simplicity and robustness
 81 of this already existing technology.

82 Gaseous CO₂ can be converted into O₂ and CO using different methods, that are
 83 the subject of a large scientific activity for applications on Earth. As a matter of fact,
 84 due to the continuous growth of fossil fuel consumption and the steady increase of an-
 85 thropogenic greenhouse gas emissions (IEA, 2019), the scientific community is actively
 86 investigating how to replace fossil fuels by solar fuels, *i.e.*, how to produce synthetic fu-
 87 els from renewable electricity, using CO₂ as a raw material. The bottleneck in this scheme
 88 is achieving an efficient CO₂ dissociation, in a process compatible with the geographic
 89 constraints and intermittency of renewable energy sources. Low-temperature plasmas
 90 provide a very interesting context to address the problem (Fridman, 2008). In this rich
 91 medium, several dissociation pathways are possible: the high-energy electrons can direct-
 92 ly dissociate the CO₂ molecule; high-power plasma sources may significantly heat
 93 the gas and enhance thermal dissociation; and in typical conditions found for operation
 94 of various discharges the electrons can efficiently transfer their energy into the vibrational
 95 excitation of CO₂, that can be subsequently up-pumped along the asymmetric stretch-
 96 ing mode to high levels and enhance dissociation via non-equilibrium processes (Fridman,
 97 2008; A. Goede & van de Sanden, 2017). The latter process is essential to achieve high
 98 energy efficiencies for CO₂ conversion, above those obtainable under thermally-driven
 99 processes. There are many other advantages of plasma technologies besides energy ef-
 100 ficiency, such as the possibility of instant start and stop of operation, scalability, and its
 101 relatively cheap design that does not require the use of scarce materials.

102 Even though CO₂ reforming is a widely discussed topic and a vast research is de-
 103 voted to it in terms of reduction of greenhouse emission, production of solar fuels and
 104 chemical materials on Earth, very few studies are available regarding the use of plasmas
 105 in Martian conditions. The suggestion to use plasmas for ISRU on Mars dates back to
 106 the 1990s in a series of papers by Outlaw and co-workers (Outlaw, 1990; Ash et al., 1994;
 107 Wu et al., 1996), with a very recent follow-up by (Premathilake et al., 2019). Alterna-
 108 tive ideas have been proposed by (Gruwenwald, 2014). Some works related to plasmas
 109 on Mars do not focus on ISRU and address, *e.g.*, the characterisation of electrical dis-
 110 charges in CO₂/Ar/N₂ mixtures (Manning et al., 2010; Garcia-Cosio et al., 2011), the
 111 study of vibrational-energy transfers in spacecraft entry conditions (Annaloro & Bultel,
 112 2019), or the calculation of cross sections (Laricchiuta et al., 2009) and transport coef-
 113 ficients (Catalfamo et al., 2009) for the dominant heavy-particles in the Martian atmo-
 114 sphere.

115 In a recent study, we have put forward a strong case for oxygen and propellant pro-
 116 duction on Mars directly from the atmosphere using low-temperature plasmas, by show-
 117 ing that Mars has nearly ideal conditions for CO₂ dissociation by plasmas (Guerra et
 118 al., 2017, 2018). In particular, it was advocated that: i) the pressure on the surface of

119 Mars (~ 4.5 Torr) is very suitable for plasma operation, since the discharge tends to be
 120 homogeneous and is easy to ignite; ii) the cold Martian atmosphere may enhance vibration-
 121 vibration (V-V) up-pumping and hinder vibration-translation (V-T) deactivation, favor-
 122 ing dissociation via the indirect route that takes advantage of vibrational non-equilibrium;
 123 iii) Ar and N₂ may shift the electron energy to higher values and help pumping the CO₂
 124 asymmetric stretching mode, respectively, contributing as well to enhance dissociation
 125 and increase its efficiency. The simulations in (Guerra et al., 2017, 2018) show very promis-
 126 ing results, but no experimental confirmation of these predictions was attempted to date.

127 Herein we undertake a joint experimental and modeling investigation to assess the
 128 validity of the ideas advanced by Guerra et al. (2017, 2018). To this purpose, experiments
 129 are carried out in plasmas created in simple and reproducible DC glow discharges, in pure
 130 CO₂ and in a synthetic Martian atmosphere of 96% of CO₂ with 2% of Ar and 2% of
 131 N₂, for pressures in the range 0.5-6 Torr, discharge currents from 20 to 50 mA, both with
 132 the input gas at room temperature (300 K) and typical Mars average temperatures (220 K).
 133 The CO₂ and CO vibrational temperatures, the conversion factor, and the gas temper-
 134 ature are measured in these conditions using *in situ* Fourier transform infrared (FTIR)
 135 spectroscopy, while the reduced electric field is determined from the voltage drop between
 136 two tungsten probes at the floating potential. The bases of the experimental set-up are
 137 similar to the ones used in former fundamental studies on CO₂ reforming on Earth (Klarenaar
 138 et al., 2017; Morillo-Candas et al., 2019). The low-temperature Martian conditions are
 139 recreated here by immersing the plasma reactor in a bath of dry ice and ethanol. To the
 140 best of our knowledge, these measurements constitute the first experimental character-
 141 ization of plasmas created in a realistic Martian environment and address, at the same
 142 time, the vibrational non-equilibrium and the CO₂ conversion in these plasmas. Prelim-
 143 inary results were presented in (Ogloblina et al., 2019).

144 To complement the experimental study, a detailed self-consistent kinetic model is
 145 developed to analyze and interpret the experimental data obtained in pure CO₂. The
 146 model describes the electron kinetics, by solving the electron Boltzmann equation for a
 147 CO₂/CO/O₂/O mixture (Grofulović et al., 2016; Ogloblina et al., 2020) using the two-
 148 term Boltzmann solver LoKI-B (Tejero-del-Caz et al., 2019), coupled with the heavy-
 149 particle kinetics, described by a set of rate balance equations for the creation and de-
 150 struction of the most important neutral and charged heavy-particles in the plasma, namely
 151 CO₂($\nu_1\nu_2^{\prime 2}\nu_3$), CO($X^1\Sigma^+, a^3\Pi_r$), O₂($X^3\Sigma_g^-, a^1\Delta_g, b^1\Sigma_g^+$), O($^3P, ^1D$), O₃, CO₂⁺, CO⁺,
 152 O₂⁺, O⁺, and O⁻, following the formulation from (Guerra & Loureiro, 1999) and imple-
 153 mented in the LoKI simulation tool as described in (Tejero-del-Caz et al., 2018; *The Lis-*
 154 *bOn KInetics - LoKI*, 2019). Here, CO₂($\nu_1\nu_2^{\prime 2}\nu_3$) accounts for 72 individual CO₂ vibra-
 155 tional levels (see section 3). This model constitutes a major improvement regarding our
 156 previous simulations for CO₂ plasmas, where only the coupling between the electron ki-
 157 netics and the CO₂($\nu_1\nu_2^{\prime 2}\nu_3$) vibrational levels is taken into account (T. Silva, Grofulović,
 158 Klarenaar, et al., 2018; Grofulović et al., 2018; T. Silva, Grofulović, Terraz, et al., 2018;
 159 T. Silva et al., 2020), or where no vibrational excited states of CO₂ are considered (A. F. Silva
 160 et al., 2020), or where vibrational states of CO₂ are included with very reduced set of
 161 chemical reactions (Morillo-Candas, Silva, et al., 2020). In addition, vibrational relax-
 162 ation of CO₂($\nu_1\nu_2^{\prime 2}\nu_3$) molecules in collisions with O atoms is now included as in (Terraz
 163 et al., 2020) and is shown to have a significant influence in shaping the CO₂ vibrational
 164 distribution functions. Vibrational relaxation in CO₂-O₂ collisions is also accounted for.

165 The structure of this paper is as follows. Section 2 briefly describes the experimen-
 166 tal setup and the diagnostics used. Section 3 details the formulation of the model and
 167 describes the input data. The experimental and modelling results are presented and dis-
 168 cussed in section 4. Finally, section 5 summarises our main findings.

2 Experiment

The experimental setup and diagnostics used are very similar to those described in (Morillo-Candas et al., 2019; Klarenaar et al., 2017). In addition, a new system had to be devised and included in the setup to reproduce the Martian low-temperature conditions, as further described below.

The plasma reactor under study is a cylindrical-shaped Pyrex tube, with a 2 cm inner diameter and a length of 23 cm. The electrodes are positioned 17 cm apart, opposite to the gas in- and outlet. The reactor is connected in series with a 40 k Ω resistor to a DC power supply. The electric field in the reactor is measured with two tungsten pins radially pointing inside the positive column of the glow discharge. The positive column can be considered homogeneous (Raizer, 1991) and, therefore, the measurement of the electric field with two pins gives the value of the average field in the whole bulk of the plasma. The discharge current is varied between 10 and 50 mA. The pressure is varied between 0.5 and 5 Torr, using a scroll pump (Edwards XDS-5), and a pressure gauge (Pfeiffer CMR263) with feedback to an automated pressure regulating valve (Pfeiffer EVR116) and controller (Pfeiffer RVC300).

The experiments are conducted both in pure CO₂ and in a synthetic Martian atmosphere corresponding to a mixture of 96% CO₂ with 2% of Ar and 2% of N₂ (all Air Liquide Alphagaz 1). The gas flows are controlled using mass flow controllers (Bronkhorst F-201CV). A total gas flow of 7.4 sccm has been used in our previous work comparing experiment with models (T. Silva, Grofulović, Klarenaar, et al., 2018; T. Silva, Grofulović, Terraz, et al., 2018; Terraz et al., 2020; A. F. Silva et al., 2020) and is employed as well as the reference condition in the present experiments. However, to insure a good precision of the concentration of the small admixtures of Ar and N₂ necessary to reproduce the Martian mixture, for the corresponding additional measurements a larger total gas flow of 19.25 sccm is used, composed of 0.39 sccm of nitrogen and 0.39 sccm of argon and the remainder of CO₂.

The reactor is positioned in the sample compartment of a FTIR spectrometer (Bruker V70) as presented in figure 1. The chosen configuration ensures that the IR absorption measurements (line-of sight-integrated) are taken only through the positive column of the glow discharge. The contribution of the IR emission from the plasma is subtracted to the transmission spectra. The detected IR spectra contain several lines of CO and CO₂ vibrational transitions and are fitted according to the procedure described by (Klarenaar et al., 2017, 2019). It is assumed that the rotational and vibrational temperatures are uniform along the length of the positive column. As an outcome of the fitting procedure, the vibrational temperatures of CO₂ and CO, the rotational temperature of CO and CO₂ - assumed to be representative of the gas temperature (Morillo-Candas et al., 2019) - , and the dissociation fraction

$$\alpha = \frac{[CO]}{[CO] + [CO_2]} ,$$

where [CO] and [CO₂] represent the gas phase concentrations of CO and CO₂ molecules, respectively, are obtained from the acquired spectra.

To mimic Mars-like temperature conditions, the reactor is immersed into a mixture of dry ice and ethanol, as shown in the photos of the setup and the discharge in figure 2. Both the mixture temperature and the gas temperature inside the reactor before igniting the plasma are controlled with a temperature dependent platinum thin film chip resistor (Vishay PTS 0603). The nominal resistance temperature specifications from the manufacturer (given down to 215 K) was cross checked by calibrating it with a chiller (Huber 230) down to 243 K. The temperature of the gas before experiencing the plasma is further controlled by the FTIR measurements and is approximately 220–230 K. Both techniques agree within a 5% error for “plasma off” gas temperature measurements. As the temperature probe sensor is an intrusive diagnostics, it is not used for the “plasma

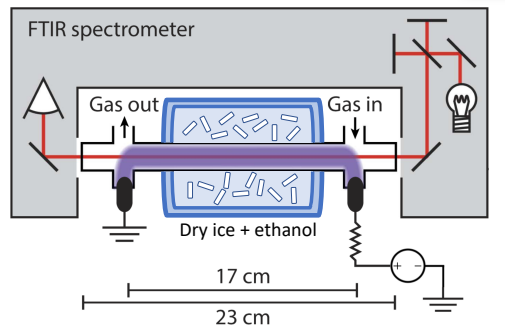


Figure 1. Schematic representation of the discharge reactor placed in the sample compartment of the FTIR spectrometer and immersed in a mixture of dry ice and ethanol. Adapted from (Klarenaar et al., 2017).

208 on” measurements and only the results obtained from the FTIR absorption spectra are
 209 considered. For the Earth temperature conditions, the same operating conditions were
 210 tested without surrounding the reactor by the dry ice and ethanol bath.



Figure 2. Discharge reactor immersed into a mixture of dry ice and ethanol and positioned in the sample compartment of the FTIR when the plasma is ON.

211 3 Model

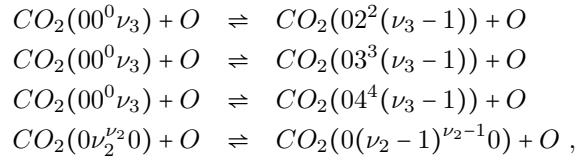
212 A self-consistent kinetic model was developed to interpret the experimental results
 213 and describe the detailed kinetics of the major species in plasmas created in DC CO₂
 214 discharges. It couples the electron, vibrational, chemical and ion kinetics, and builds on
 215 previous models for CO₂-containing plasmas, already tested and validated in discharges
 216 and afterglows and for various operating conditions (T. Silva, Grofulović, Klarenaar, et
 217 al., 2018; Grofulović et al., 2018; T. Silva, Grofulović, Terraz, et al., 2018; Terraz et al.,
 218 2020; T. Silva et al., 2020; A. F. Silva et al., 2020). The model takes as input the pa-
 219 rameters controlled in a real experiment, in particular the discharge current, I , pressure,
 220 p , gas flow, Φ , and tube radius, R . Additionally, in the present simulations the gas tem-
 221 perature, T_g , is also given as an input parameter, since its value is available from exper-
 222 iment and our purpose is not to focus on the gas heating mechanisms but rather on the
 223 plasma chemistry in the system. Note that the gas thermal balance equation can be in-
 224 corporated in the present formulation, as it was already done in (T. Silva et al., 2020).

225 The EEDF is obtained from the solution of the homogeneous and stationary elec-
 226 tron Boltzmann equation in a CO₂/CO/O₂/O mixture, solved in the usual two-term ex-
 227 pansion in Legendre polynomials. The calculations are done with the LisbOn KInetics
 228 Boltzmann solver LoKI-B (Tejero-del-Caz et al., 2018; *The LisbOn KInetics - LoKI*, 2019),
 229 an in-house code developed in object-oriented programming under MATLAB[®] and dis-
 230 tributed in open source. The electron impact cross sections for the different gases have
 231 been previously validated and are described in (Grofulović et al., 2016) for CO₂, (Ogloblina
 232 et al., 2020) for CO, and in (Alves et al., 2016) for O₂ and O, and can be obtained from
 233 IST-Lisbon database at the open-access web-platform LXCat (*Plasma Data Exchange*
 234 *Project*, 2010). These cross sections have been mostly based on (Lowke et al., 1973; Ce-
 235 liberto et al., 2014, 2016) for CO₂, (Itikawa, 2015; Laporta et al., 2012; Sawada et al.,
 236 1972; Rapp & Briglia, 1965; Rapp & Englander-Golden, 1965; Cosby, 1993) for CO, (Phelps,
 237 1985; Lawton & Phelps, 1978) for O₂ and (Laher & Gilmore, 1990) for O. The EEDF
 238 is calculated taken into account elastic and inelastic collisions of electrons with the par-
 239 ent gases, whose concentrations are self-consistently calculated (see below), as well as
 240 stepwise and superelastic collisions with vibrationally excited CO₂ and CO molecules
 241 and electronically excited metastables molecules O₂(a, b) and CO(a) and atoms O(¹ D).

242 The electron Boltzmann equation is coupled to a system of rate balance equations
 243 describing the creation and loss of neutral and charged heavy-species, using the approach
 244 from (Guerra & Loureiro, 1997, 1999). The resulting global model is simulated with the
 245 LoKI simulation tool (Tejero-del-Caz et al., 2018; *The LisbOn KInetics - LoKI*, 2019).
 246 The species considered in the model include: 72 vibrationally excited CO₂ levels, rep-
 247 resented as CO₂($\nu_1\nu_2^l\nu_3$), where $\nu_1 \leq 2$, $\nu_2 \leq 5$ and $\nu_3 \leq 5$ denote the vibrational quanta
 248 in the symmetric stretching, bending, and asymmetric stretching vibrational modes, re-
 249 spectively, and l_2 defines the projection of the angular momentum of bending vibrations
 250 onto the axis of the molecule (T. Silva, Grofulović, Klarenaar, et al., 2018); ground-state
 251 and electronically excited CO and O₂ molecules, CO($X^1\Sigma^+, a^3\Pi_r$), O₂($X^3\Sigma_g^-, a^1\Delta_g, b^1\Sigma_g^+$);
 252 ground-state and electronically excited oxygen atoms, O(³ $P, ^1D$); ground-state and vi-
 253 brationally excited ozone, O₃ and O₃^{*}, respectively; and positive and negative ions, CO₂⁺,
 254 CO⁺, O₂⁺, O⁺, and O⁻. Following the results in (Morillo-Candas, Silva, et al., 2020), elec-
 255 tron impact dissociation from ground-state CO₂(00⁰) molecules is taken into account
 256 using the dissociation cross section from Polak and Slovetsky (1976). As discussed in (Grofulović
 257 et al., 2016), this cross section is not part of the complete and consistent CO₂ cross sec-
 258 tion set and, accordingly, is not used to obtain the EEDF, but is integrated with the cal-
 259 culated EEDF to obtain the corresponding rate coefficient. Due to the lack of data, the
 260 dissociation cross section from vibrationally excited states is considered with a thresh-
 261 old reduction, while keeping the same shape and magnitude as for dissociation from the
 262 ground-state. The same threshold reduction procedure is used to account for ionization
 263 from vibrationally excited CO₂ molecules. The loss probability of O atoms at the wall,

264 γ_O , is considered with the expression proposed by Morillo-Candas et al. (2019), deduced
 265 from the experimental determination of O-atom loss frequencies. The details on the com-
 266 plex plasma chemistry taken into account can be found in previous publications deal-
 267 ing with the CO₂ vibrational kinetics (T. Silva, Grofulović, Klarenaar, et al., 2018; Gro-
 268 fulović et al., 2018), the kinetic mechanisms in O₂ plasmas (Annušová et al., 2018), and
 269 the plasma chemistry in vibrationally cold CO₂ (A. F. Silva et al., 2020).

270 Note that no chemistry was included in (T. Silva, Grofulović, Klarenaar, et al., 2018;
 271 Grofulović et al., 2018), a reduced chemistry set with only five reactions was coupled with
 272 the vibrational kinetics in (Morillo-Candas, Silva, et al., 2020), while no vibrational ki-
 273 netics was considered in (A. F. Silva et al., 2020). Accordingly, the current model con-
 274 stitutes a significant upgrade of our prior models, by describing self-consistently and in
 275 detail the coupled electron, vibrational and chemical kinetics. Moreover, T. Silva, Gro-
 276 fulović, Klarenaar, et al. (2018); Grofulović et al. (2018) only consider vibrational en-
 277 ergy transfers in CO₂-CO₂ collisions and vibrational deactivation at the wall, as they
 278 focused in the so-called ‘single-pulse’ experiment, where CO₂ dissociation is very low.
 279 However, in a steady-state situation, significant amounts of CO, O₂ and O are present
 280 in the plasma (*cf.* section 4). Therefore, we have additionally included vibrational-to-
 281 translation (VT) energy exchanges in CO₂-O collisions:



282 as they can affect significantly the vibrational distribution functions even for relatively
 283 small amounts of atomic oxygen (Terraz et al., 2020; Morillo-Candas, Klarenaar, et al.,
 284 2020). The corresponding rate coefficients are given by López-Puertas et al. (1986) for
 285 $\nu_2 = 1$ and $\nu_3 = 1$ and the harmonic oscillator scaling (linear with ν_2 or ν_3) is assumed
 286 for $\nu_2, \nu_3 > 1$. CO₂-O₂ VT processes are further included according to López-Puertas
 287 et al. (1986). However, for the present conditions their influence is much smaller than
 288 the quenching by atomic oxygen.

289 Some of the most important reactions considered in the model are listed in Table
 290 1 alongside with corresponding references. This is by no means an exhaustive list and
 291 its main purpose is to guide the discussion in section 4. The reader should refer to our
 292 publications (T. Silva, Grofulović, Klarenaar, et al., 2018; Grofulović et al., 2018; Annušová
 293 et al., 2018; A. F. Silva et al., 2020) for a complete kinetic scheme. The rate coefficients
 294 for the heavy-particle reactions involving the metastable state CO(*a* ³Π_r) are discussed
 295 in (A. F. Silva et al., 2020). The rate coefficient for CO₂ dissociation in collisions involv-
 296 ing vibrationally excited CO₂($\nu_1\nu_2^l\nu_3$) and CO(*a*), reaction R3c, is considered with the
 297 same rate coefficient as for ground-state CO₂, reaction R3b.

298 The self-consistent sustaining reduced electric field, E/N , is obtained as an eigen-
 299 value to the problem, from the requirement that, under steady-state conditions, the to-
 300 tal rate of production of electrons in ionization events must compensate exactly their to-
 301 tal loss rate due to ambipolar diffusion and electron-ion recombination, while respect-
 302 ing quasi-neutrality (Guerra & Loureiro, 1997, 1999). A generic flowchart of the algo-
 303 rithm used to couple the electron, neutral, and ion kinetics, is presented in (Guerra et
 304 al., 2002) and an updated scheme is available at the LoKI website (*The LisbOn KInet-*
 305 *ics - LoKI*, 2019).

306 4 Results and Discussion

307 This section presents and analyses the experimental and simulation results in con-
 308 tinuous DC discharges at pressures $p = 0.5\text{--}5$ Torr, discharge currents $I = \{20, 50\}$ mA,

Table 1. List of some important reactions mentioned in the text.

R1a	$CO(a) + O_2(X) \rightarrow CO(X) + O(^3P) + O(^3P)$	(A. F. Silva et al., 2020)
R1b	$CO(a) + O_2(X) \rightarrow CO(X) + O_2(X)$	(A. F. Silva et al., 2020)
R2	$CO(a) + CO(X) \rightarrow CO(X) + CO(X)$	(A. F. Silva et al., 2020)
R3a	$CO(a) + CO_2 \rightarrow CO(X) + CO_2$	(A. F. Silva et al., 2020)
R3b	$CO(a) + CO_2(00^0_0) \rightarrow CO(X) + CO(X) + O(^3P)$	(A. F. Silva et al., 2020)
R3c	$CO(a) + CO_2(\nu_1\nu_2^{\prime 1/2}\nu_3) \rightarrow CO(X) + CO(X) + O(^3P)$	see text
R4	$CO(a) + O(^3P) \rightarrow CO(X) + O(^3P)$	(Shofield, 1979)
R5	$e + CO_2(00^0_0) \rightarrow e + CO(X) + O(^1D)$	(Grofulović et al., 2016)
R6a	$e + CO_2(01^1_0) \rightarrow e + CO(X) + O(^1D)$	(Grofulović et al., 2016)
R6b	$e + CO_2(02^2_0) \rightarrow e + CO(X) + O(^1D)$	(Grofulović et al., 2016)
R6c	$e + CO_2(10^0_0 + 02^0_0) \rightarrow e + CO(X) + O(^1D)$	(Grofulović et al., 2016)
R7	$O^- + CO(X) \rightarrow e + CO_2(00^0_0)$	(A. F. Silva et al., 2020)
R8	$e + CO(X) \rightleftharpoons e + CO(a)$	(Ogloblina et al., 2020)
R9	$CO(a) + O_2(X) \rightarrow CO_2(00^0_0) + O(^3P)$	(A. F. Silva et al., 2020)
R10	$e + CO_2(00^0_0) \rightarrow CO(X) + O^-$	(Grofulović et al., 2016)
R11	$O_2(b) + O(^3P) \rightarrow O_2(X) + O(^3P)$	(Annušová et al., 2018)
R12	$O_2(a) + \text{wall} \rightarrow O_2(X)$	(Annušová et al., 2018)
R13	$O_2(b) + \text{wall} \rightarrow O_2(X)$	(Annušová et al., 2018)
R14	$O(^3P) + \text{wall} \rightarrow 0.5O_2(X)$	(Morillo-Candas et al., 2019)
R15	$e + O_2(X) \rightleftharpoons e + O_2(a)$	(Annušová et al., 2018)
R16	$e + O_2(X) \rightleftharpoons e + O_2(b)$	(Annušová et al., 2018)
R17	$e + O_2(X) \rightarrow e + O(^3P) + O(^3P)$	(Annušová et al., 2018)
R18	$e + O_2(X) \rightarrow e + O(^3P) + O(^1D)$	(Annušová et al., 2018)
R19	$O(^1D) + O_2(X) \rightarrow O(^3P) + O_2(b)$	(Annušová et al., 2018)

309 addressing: *i*) the differences induced by Earth and Mars atmospheric temperature con-
 310 ditions in the plasma chemistry in pure CO₂ (section 4.1); *ii*) the influence of the am-
 311 bient temperature on the vibrational kinetics of CO₂ (section 4.2); *iii*) the effect of the
 312 Mars atmospheric minor constituents N₂ and Ar in CO₂ decomposition (section 4.3). The
 313 total gas flow is $\Phi = 7.4$ sccm for i) and ii) and $\Phi = 19.25$ sccm for iii).

314 4.1 CO₂ plasma chemistry at Mars and Earth temperature conditions

315 We first investigate the influence of the ambient temperature on the plasma chem-
 316 istry in pure CO₂ plasmas, while keeping the pressure around the Martian atmospheric
 317 pressure. For this purpose, we compare the results obtained when the plasma is ignited
 318 at Martian (~ 220 K) or Terrestrial (~ 300 K) ambient temperatures, in order to find
 319 out up to which extent the results obtained on Earth at low pressure can be assumed
 320 to be valid on Mars.

321 Figure 3 shows the measured and calculated values of the reduced electric field, E/N ,
 322 as a function of the gas density (N) \times tube radius (R) product for currents $I = 20$ mA
 323 and 50 mA. The E/N values are deduced from two independent measurements: on the
 324 one hand, from the electric field evaluation performed by measuring the floating poten-
 325 tial of two tungsten pins inserted in the positive column; and, on the other hand, from
 326 the measurement of the gas temperature from which the gas density is deduced via the
 327 ideal gas law (*cf.* section 2). A true statistical study of reproducibility on these two mea-
 328 surements was not carried out and the error bars shown are only an upper value esti-
 329 mate based on the cumulative errors of these two measurements. The corresponding val-
 330 ues of the gas temperature, T_g , obtained from the FTIR measurements of the rotational
 331 distribution of CO₂ and CO, are given in Table 2. The gas heating induced by plasma

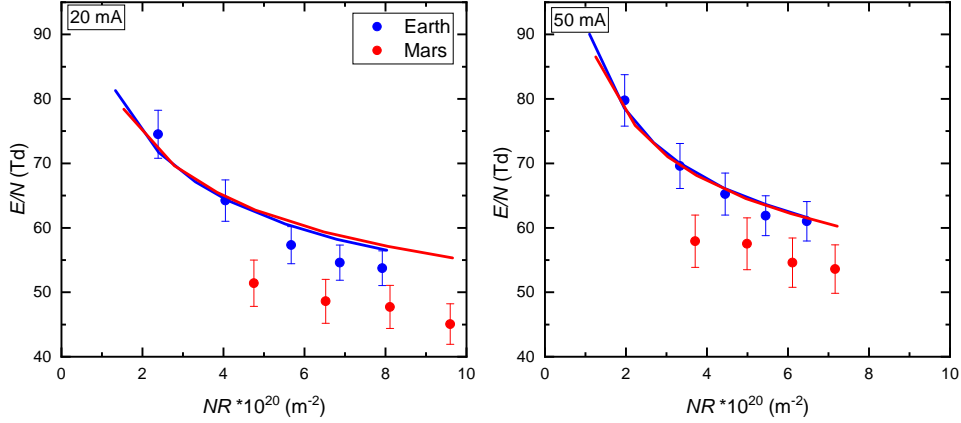


Figure 3. Reduced electric field, E/N , as a function of the NR product, when a pure CO_2 discharge is ignited at **Mars** and **Earth** background temperatures at currents $I = 20$ mA (left panel) and $I = 50$ mA (right panel): experiment (\bullet), self-consistent calculation ($—$).

332 remains very similar for both Mars and Earth conditions and, therefore, the gas tem-
 333 perature for all conditions is essentially shifted from Mars to Earth by an offset typically
 334 around 70-80 K. Three notes are worth making. First, there is an excellent agreement
 335 between measurements and simulations in Earth conditions. Second, the experimental
 336 results show that an increase in the discharge current induces a small raise in the value
 337 of E/N . This behavior is well captured in the simulations and is partially due to the eas-
 338 ier ionization of CO_2 as compared with CO (Ogloblina et al., 2020) and to the increase
 339 of the dissociation of CO_2 with the discharge current (see Figure 4), as discussed in (A. F. Silva
 340 et al., 2020). Finally, the measurements further show that the Martian conditions lead
 341 to slightly lower values of the reduced electric field than on Earth, although no notice-
 342 able variation is found in the self-consistent calculations. These small differences in mag-
 343 nitude between model predictions and measurements in Martian conditions suggest that
 344 some details of the charged particle kinetics may be missing in the model, such as tem-
 345 perature dependencies of some rate coefficients, or that improved charged-particle trans-
 346 port data are needed. Overall, the self-consistent calculations of the reduced electric field
 347 are in very satisfactory agreement with experiment and the results show that the model
 348 can be used as a predictive tool when no experimental data for E/N are available. Here,
 349 to avoid an error propagation in the analysis, the experimental values of E/N are given
 350 as input to the simulations shown in the remainder of the paper.

351 The measured and calculated CO_2 dissociation fractions, $\alpha = [\text{CO}]/([\text{CO}]+[\text{CO}_2])$,
 352 are represented in Figure 4. To assess the role of the vibrationally excited states, the cal-
 353 culations are performed both considering (full curves) and neglecting (dashed curves)
 354 the vibrational kinetics in the model. Additional simulations are carried out to evalu-
 355 ate the importance of superelastic collisions with vibrationally excited states in shap-
 356 ing the EEDF, by giving the experimental populations of vibrationally excited CO and
 357 CO_2 molecules as input to the electron Boltzmann solver, while no vibrationally excited
 358 states are considered in the system of rate balance equations for the heavy-particles (dot-
 359 ted curves). There is a quite good agreement between the model predictions and the ex-
 360 perimental data. The inclusion of the vibrational kinetics increases the calculated dis-
 361 sociation fraction, as a result of two effects: the modifications of the EEDF due to su-
 362 perelastic collisions with vibrationally excited CO and CO_2 , which enhance the high energy-
 363 tail (Ogloblina et al., 2020; Pietanza et al., 2020), and correspond to the differences be-

Table 2. Measured gas temperature (K) deduced from rotational temperature of CO and CO₂ in pure CO₂ plasmas

	20 mA		50 mA	
p (Torr)	Mars	Earth	Mars	Earth
0.5	309	390	380	430
1	348	405	425	490
1.5	378	463	485	555
2	406	477	520	580
3	444	511	580	651
4	476	562	632	709
5	503	610	674	747

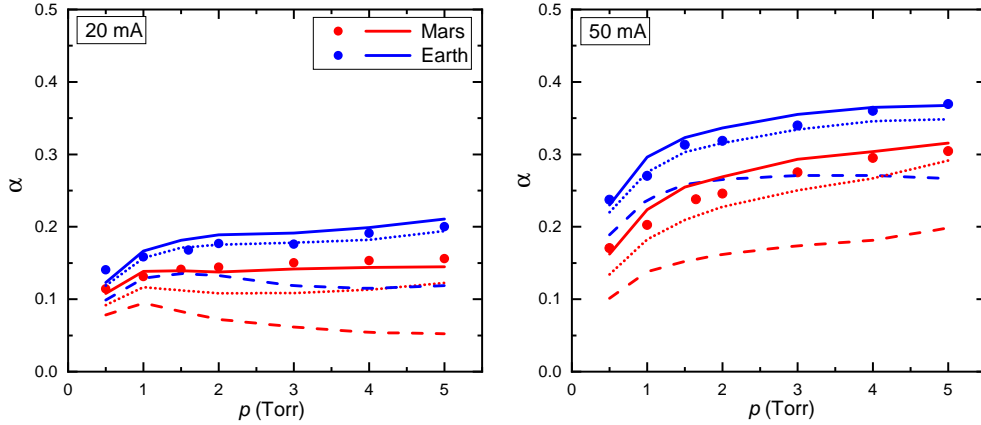


Figure 4. CO₂ dissociation fraction when a pure CO₂ discharge is ignited at Mars and Earth background temperatures at currents $I = 20$ mA (left panel) and $I = 50$ mA (right panel): experiment (\bullet), model calculations by including (—) and excluding (---) the vibrational kinetics, and by considering the influence of vibrational excited states only in the electron Boltzmann equation (\cdots).

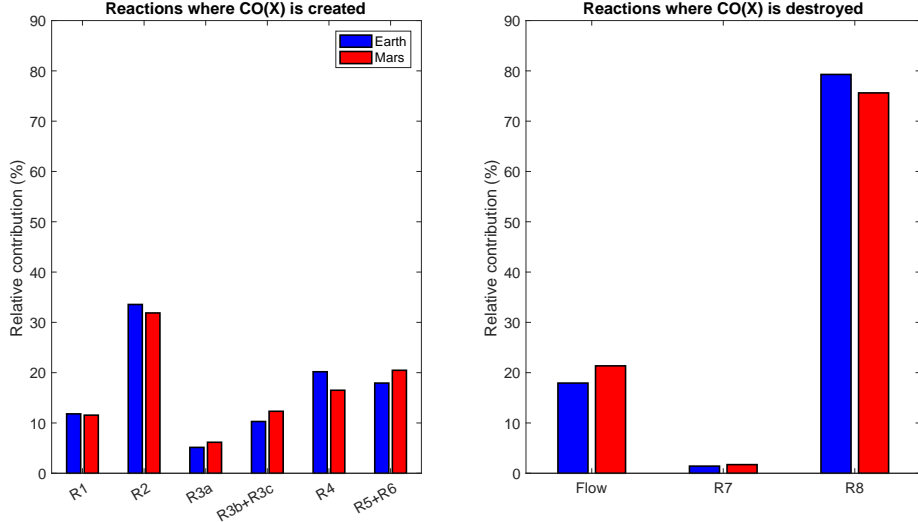


Figure 5. Relative contribution (in %) of the main mechanisms of creation and destruction of $\text{CO}(X^1\Sigma^+)$ when a pure CO_2 discharge at $p = 5$ Torr and $I = 50$ mA is ignited at **Mars** and **Earth** background temperatures. The reactions are identified in Table 1.

364 between the dashed and dotted curves; the contribution of the vibrational states of CO_2
 365 to dissociation by electron impact, reactions (R6), since the rate coefficients for electron-
 366 impact dissociation from the vibrationally excited states are higher than from the ground
 367 states, corresponding to the differences between the dotted and full curves. Note that
 368 the fractional population of the $\text{CO}_2(00^00)$ level can be as low as 0.45 (see below), and
 369 the corresponding dissociation rate coefficient can be up to 1.7 and 5.6 times smaller than
 370 from the (01^10) and the (02^20) levels, respectively. Superelastic collisions have a promi-
 371 nent role in all conditions. In turn, the influence of dissociation from vibrationally ex-
 372 cited CO_2 is quite significant on Martian conditions and is relatively small on Earth, due
 373 to the lower values of E/N in the former case. Dissociation fractions in the range 10-
 374 30% are observed for Martian temperature conditions, which is a promising result re-
 375 garding the use of plasma technologies for ISRU on Mars, specially taking into account
 376 that the present reactor was designed for fundamental studies and is far from any plasma
 377 system to be used in a prototype.

378 Figure 5 quantifies the contribution of the different creation and destruction mech-
 379 anisms of $\text{CO}(X^1\Sigma^+)$ molecules for $p = 5$ Torr and $I = 50$ mA. Reactions R1 and R6
 380 in the figure correspond to the total contributions identified in Table 1, $\text{R1} = \text{R1a} + \text{R1b}$,
 381 $\text{R6} = \text{R6a} + \text{R6b} + \text{R6c}$. In these conditions, the relative populations of levels (00^00) , (01^10) ,
 382 (02^20) and $(10^00 + 02^00)$ are 0.453, 0.254, 0.071 and 0.072, respectively. Overall, the domi-
 383 nant mechanisms on Mars and Earth conditions are quite similar. According to the simu-
 384 lations, ground-state $\text{CO}(X^1\Sigma^+)$ molecules are essentially created by dissociation by
 385 electron impact on $\text{CO}_2(\nu_1\nu_2^l\nu_3)$ molecules, mainly on the (00^00) , (01^10) , (02^20) and
 386 the Fermi $(10^00 + 02^00)$ states (reactions R5 and R6 in Table 1), and by the quenching
 387 of the $\text{CO}(a^3\Pi_r)$ state. The latter mechanism has to be looked at with caution, as the
 388 excitation of $\text{CO}(a^3\Pi_r)$ from ground-state $\text{CO}(X^1\Sigma^+)$ is also one of the main processes
 389 of destruction of $\text{CO}(X^1\Sigma^+)$, so that reactions involving only $\text{CO}(X)$ and $\text{CO}(a)$ do not
 390 constitute true creation/destruction mechanisms of CO molecules, but rather redistribute
 391 its population between the two electronic levels. Nevertheless, processes R3b and R3c
 392 do constitute effective creation mechanisms of CO molecules from dissociation of CO_2 in
 393 collisions with $\text{CO}(a^3\Pi_r)$ and have a significant contribution to the production of CO .

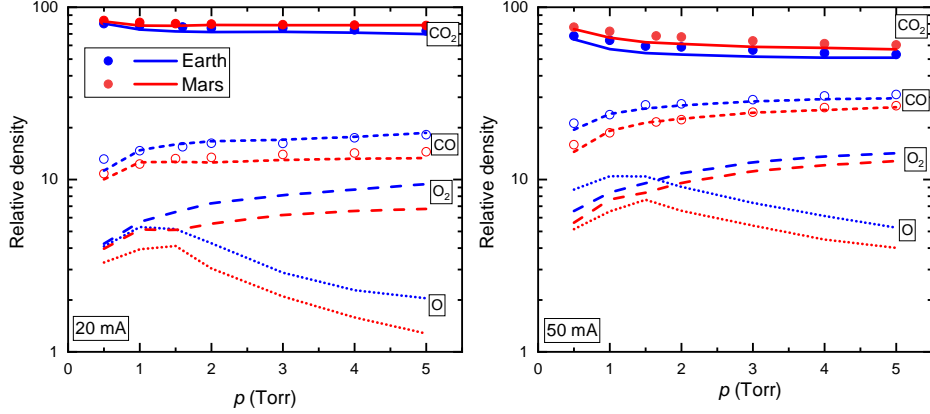


Figure 6. Relative density of the dominant species when a pure CO_2 discharge is ignited at Mars and Earth background temperatures at currents $I = 20$ mA (left panel) and $I = 50$ mA (right panel). The symbols correspond to experimental data for CO_2 (\bullet) and CO (\circ).

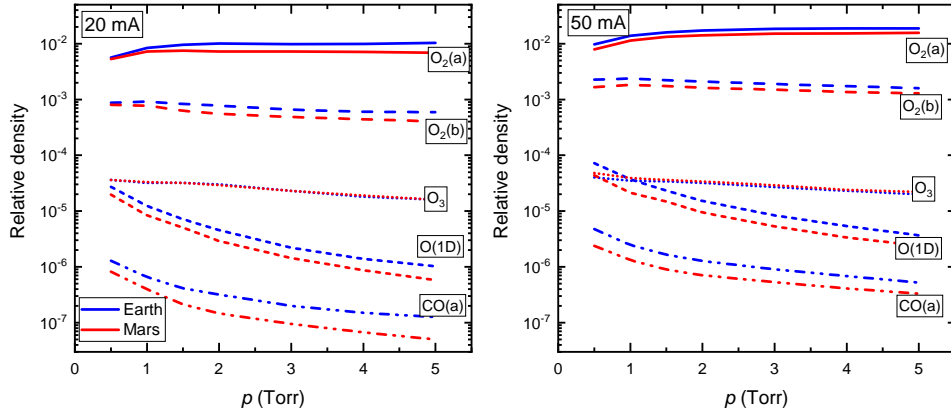


Figure 7. Relative density of various electronically excited states and of ozone, when a pure CO_2 discharge is ignited at Mars and Earth background temperatures at currents $I = 20$ mA (left panel) and $I = 50$ mA (right panel).

394 Additional destruction mechanisms of $\text{CO}(X^1\Sigma^+)$ worth mentioning are the transport
 395 by the gas flow and the electron-ion recombination reaction R7.

396 Figures 6-8 show, respectively, the calculated concentrations of the dominant neu-
 397 tral species, electronically-excited states and O_3 , and the charged particles. The den-
 398 sities represented in Figure 6 are the total densities of the parent species, *i.e.*, the sum of
 399 the populations of all the electronically metastable states; note that for CO_2 , CO and
 400 O , more than 99.9% of the total population is in the ground electronic state, while for
 401 O_2 up to $\sim 20\%$ of the population can be in the $\text{O}_2(a^1\Delta_g, b^1\Sigma_g^+)$ excited states. Ex-
 402 perimental data for CO_2 and CO are also plotted in Figure 6.

403 Most species represented in Figures 6-8 follow the trend expected by a production
 404 dictated by electron-impact dominant mechanisms (A. F. Silva et al., 2020), with a de-
 405 crease with pressure and an increase with current, as an outcome of the lower reduced
 406 electric field (and corresponding lower electron impact rate coefficients) and higher elec-

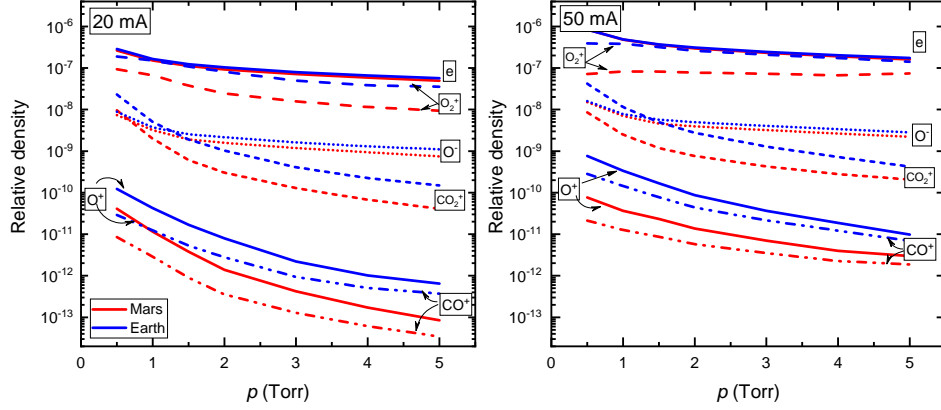
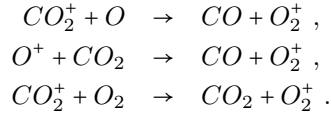


Figure 8. Relative density of various charged particles, when a pure CO_2 discharge is ignited at Mars and Earth background temperatures at currents $I = 20$ mA (left panel) and $I = 50$ mA (right panel).

407 tron density, respectively. A noticeable and important exception to this trend is CO, whose
 408 relative concentration remains nearly constant for pressures above ~ 1.5 Torr, although
 409 it is mainly produced by electron impact. The increasing behavior of O_2 is partially due
 410 to the shift from O to O_2 as the pressure increases and the associated reduction in the
 411 total number of particles. The shift in the relative concentrations of O and O_2 with pres-
 412 sure is mainly a consequence of the increase of the recombination probability of O atoms
 413 at the wall with pressure (Morillo-Candas et al., 2019), as surface recombination is the
 414 main destruction mechanism of O atoms for the present conditions. The O atom den-
 415 sities for the Earth input gas temperature are in a good agreement with the values ob-
 416 tained in (Morillo-Candas et al., 2019). It is also worth noting that O_2^+ is always the dom-
 417 inant ionic species, due to the efficient charge transfer processes from CO_2^+ and O^+ to
 418 O_2^+ , namely,



419 Further insight into the complex coupled kinetics taking place in the plasma is given
 420 by inspection of figures 9 and 10. Figure 9 displays the relative contribution of the dom-
 421 inant creation and destruction mechanisms of O_2 , for the same conditions as in Figure
 422 5, $p = 5$ Torr and $I = 50$ mA. Most of the mechanisms include the excitation from $\text{O}_2(X^3\Sigma_g^-)$
 423 to $\text{O}_2(a^1\Delta_g)$ or $\text{O}_2(b^1\Sigma_g^+)$, or the de-excitation from these excited metastable states
 424 back to ground-state. Therefore, they essentially redistribute the population among the
 425 three O_2 electronic states. Exceptions are the mechanisms of wall recombination of O
 426 atoms (R14), dissociation of O_2 (R17,R18) and dissociation due to the quenching of $\text{CO}(a^3\Pi_r)$
 427 (R1a), which, therefore, play a significant role in the kinetics.

428 Figure 10 depicts the relative contribution of the dominant destruction mechanisms
 429 of the $\text{CO}(a^3\Pi_r)$ electronically excited state. $\text{CO}(a^3\Pi_r)$ is predominantly quenched to
 430 $\text{CO}(X^1\Sigma^+)$ in collisions with O_2 , CO, CO_2 and O, in mechanisms that do not lead to
 431 a destruction of a CO molecule. Similarly, it is created by direct electron impact on $\text{CO}(X^1\Sigma^+)$
 432 (R8). An effective destruction mechanism of CO molecules is reaction (R9), a back re-
 433 action mechanism involving $\text{CO}(a^3\Pi_r)$ and O_2 giving back CO_2 , recently evinced by Morillo-Candas
 434 (2019); Morillo-Candas, Guerra, and Guaitella (2020). It contributes about 1% to the

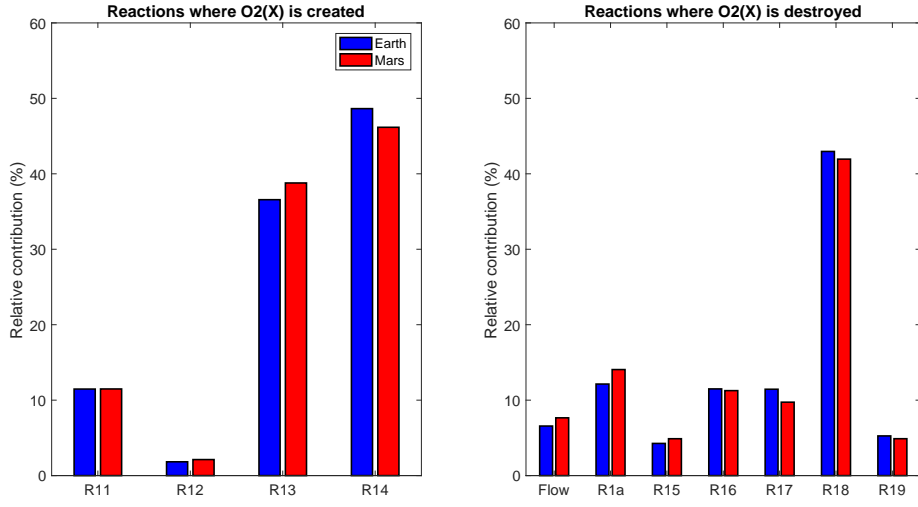


Figure 9. Relative contribution (in %) of the main mechanisms of creation and destruction of $O_2(X^3\Sigma_g^-)$ when a pure CO_2 discharge is ignited at $p = 5$ Torr and $I = 50$ mA at **Mars** and **Earth** background temperatures. The reactions are identified in Table 1.

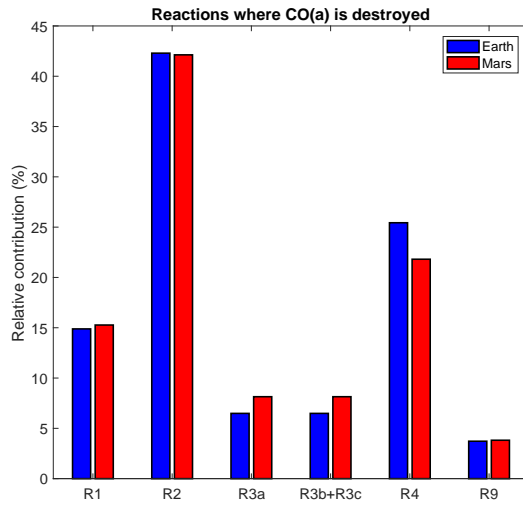


Figure 10. Relative contribution (in %) of the main mechanisms of destruction of $CO(a^3\Pi_r)$ when a pure CO_2 discharge is ignited at $p = 5$ Torr and $I = 50$ mA at **Mars** and **Earth** background temperatures. The reactions are identified in Table 1.

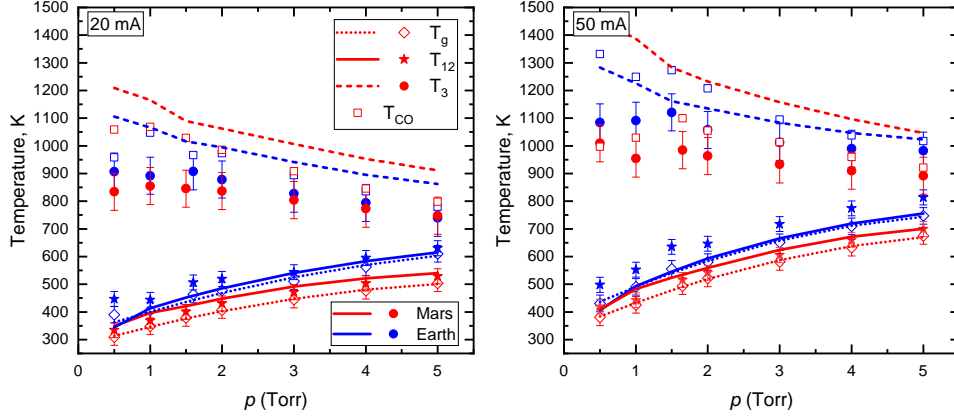


Figure 11. Experimental value of the gas temperature T_g ($\cdot \diamond \cdot$), together with the measured (symbols) and calculated (lines) vibrational temperatures of the asymmetric stretching mode T_3 (\bullet , $- -$) and the common temperature of the bending and symmetric modes T_{12} (\star , $-$) and CO vibrational temperature T_{CO} (*square*), when a pure CO_2 discharge is ignited at **Mars** and **Earth** background temperatures at currents $I = 20$ mA (left panel) and $I = 50$ mA (right panel).

435 destruction of the $\text{CO}(a^3\Pi_r)$ state, but its actual importance should not be underes-
 436 timated, as it brings an exit path from the CO manifold.

437 It is worth noting the prevalence of processes involving electronically excited states,
 438 $\text{O}_2(a^1\Delta_g)$, $\text{O}_2(b^1\Sigma_g^+)$, $\text{O}(^1D)$ and $\text{CO}(a^3\Pi_r)$, in the overall kinetics. This remark is
 439 particularly striking for the cases of $\text{O}(^1D)$ and $\text{CO}(a^3\Pi_r)$, whose relative densities are
 440 rather low, as it can be seen in Figure 7. Nonetheless, the results reveal a strong cou-
 441 pling between the kinetics of all these electronically excited states and the parent atoms
 442 and molecules. Similar conclusions have been drawn for oxygen plasmas in (Annušová
 443 et al., 2018). A more detailed analysis of the plasma chemistry in CO_2 -containing dis-
 444 charges will be presented in future publications.

445 4.2 CO_2 vibrational kinetics at Mars and Earth temperature conditions

446 One argument advanced in (Guerra et al., 2017, 2018) in favor of ISRU on Mars
 447 by plasmas was the increased degree of vibrational non-equilibrium that would be pro-
 448 moted by the ambient conditions on the red planet. In appropriate discharge configu-
 449 rations, such as radio-frequency, microwave or gliding arc discharges, it might be possi-
 450 ble to benefit from the energy stored in the vibrational levels to enhance the energy
 451 efficiency of CO_2 dissociation (Fridman, 2008). In the DC glow discharges under study,
 452 CO_2 dissociation proceeds mainly by direct electron impact, with a small to negligible
 453 contribution from purely vibrational mechanisms (Morillo-Candas, Silva, et al., 2020; Morillo-Candas,
 454 Guerra, & Guaitella, 2020). Nevertheless, it is very instructive to verify the validity of
 455 the conjecture in (Guerra et al., 2017, 2018), to guide the development of plasmas sources
 456 designed for ISRU on Mars, as well as to further analyze the results in Figure 4.

457 Figure 11 represents the measured gas temperature, T_g , the vibrational temper-
 458 ature of the asymmetric stretching mode, T_3 , the common temperature of the bending
 459 and symmetric stretching modes, T_{12} , and the vibrational temperature of CO, T_{CO} , to-
 460 gether with the model predictions for CO_2 “vibrational temperatures.” The CO vibra-
 461 tional temperature is taken into account as an input parameter for the EEDF calcula-
 462 tion, but CO vibrations are not accounted for in the chemistry module and, thus, are

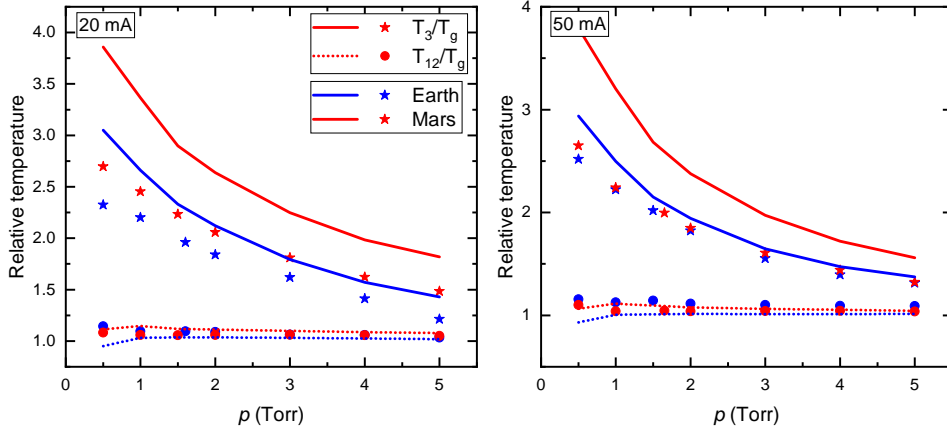


Figure 12. Measured (symbols) and calculated (lines) ratios T_3/T_g (—,★) and T_{12}/T_g (⋯,●) when a pure CO_2 discharge is ignited at **Mars** and **Earth** background temperatures at currents $I = 20$ mA (left panel) and $I = 50$ mA (right panel).

463 not calculated in the model. It is worth emphasizing that the current state-to-state model
 464 provides the populations of the individual vibrational levels of the CO_2 molecules. There-
 465 fore, the “vibrational temperatures” correspond to the fitting of the individual popula-
 466 tions to Treanor distributions. Moreover, the fact that the bending and symmetric stretch-
 467 ing modes can be described by a common “temperature” in these conditions is not an
 468 imposition of the model but rather an outcome of the simulations, as also pointed out
 469 in (Grofulović et al., 2018). Additional details on the fitting of the individual popula-
 470 tions to the corresponding distributions are given in (Grofulović et al., 2018; T. Silva,
 471 Grofulović, Klarenaar, et al., 2018), where some vibrational distribution functions are
 472 presented. The simulations describe satisfactorily the trend and magnitude of the ob-
 473 served T_{12} and T_3 , whose values do not change significantly from a discharge ignited in
 474 Martian or Earthly ambient temperatures. The model predicts a slightly larger vibra-
 475 tional temperature of the asymmetric stretching mode on Mars than on Earth, that is
 476 not confirmed experimentally. This discrepancy is likely due to the simplified vibrational
 477 kinetics considered here concerning energy transfers between CO_2 and the dissociation
 478 products, O, O_2 and CO, that only accounts for very few VT collisions of vibrationally
 479 excited CO_2 with O atoms and disregards collisions with O_2 and CO (see section 3). In
 480 any case, the main effects seem to be already captured with the present model. The vari-
 481 ations of T_3 with pressure and current are similar to the ones reported and discussed in
 482 detail by Morillo-Candas (Morillo-Candas, 2019) for Earth conditions. They further con-
 483 firm the interest of the Martian pressure range to benefit from vibrational non-equilibrium
 484 to decompose CO_2 .

One interesting phenomenon revealed by Figure 11 is a small increase of the de-
 gree of vibrational non-equilibrium when passing from Earth to Mars, as predicted the-
 oretically in (Guerra et al., 2017). This effect is more clearly exhibited in Figure 12, which
 shows the ratios T_3/T_g and T_{12}/T_g , characterizing the degree of non-equilibrium in the
 plasma (Guerra et al., 2017, 2018). It can be verified that the common temperature of
 the bending and symmetric stretching modes remains always nearly in equilibrium with
 the gas temperature. On the contrary, the asymmetric stretching mode, of major inter-
 est for vibrationally-driven dissociation (Fridman, 2008), is clearly out of equilibrium,
 with a bigger departure from equilibrium in Martian conditions than on Earth, but only

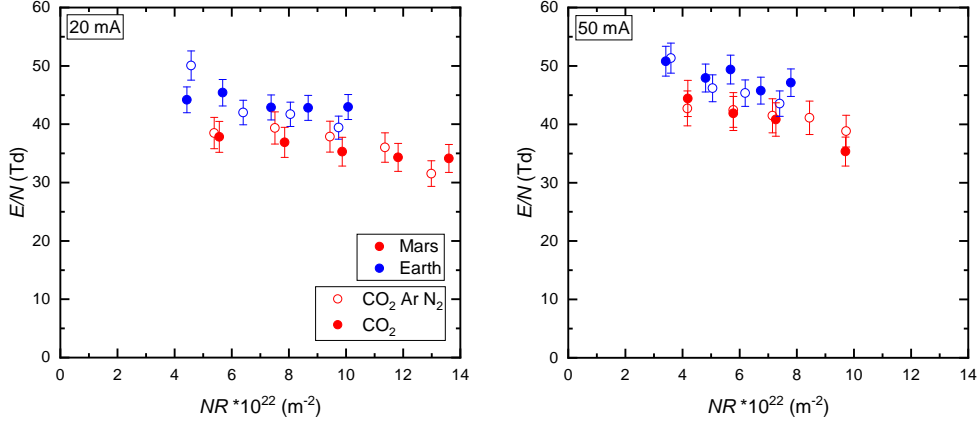
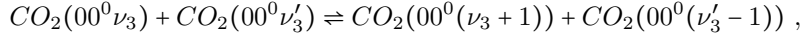


Figure 13. Reduced electric field, E/N , as a function of the NR product, measured when pure CO_2 (\bullet) and 96% CO_2 -2% Ar -2% N_2 (\circ) discharges are ignited at **Mars** and **Earth** background temperatures at currents $I = 20$ mA (left panel) and $I = 50$ mA (right panel).

for the lower current, $I = 20$ mA. In this case, the ratio T_3/T_g is always 25–30% higher on Mars than on Earth. This behavior is the outcome of the enhanced up-pumping along the asymmetric stretching mode as the temperature decreases,



485 since in the present temperature domain this VV interaction is dominated by long-range
 486 attractive forces (Pack, 1980), and of the decrease of the deactivation in VT mechanisms,
 487 dominated by short range repulsive forces. A somewhat similar effect is predicted from
 488 the model for $I = 50$ mA but is not confirmed experimentally. As noted above, these
 489 differences might stem from the simplified vibrational kinetics included in the model.

4.3 Synthetic Martian atmosphere

490 This section addresses the experimental investigation of the influence of the minor
 491 constituents of the Martian atmosphere, Ar and N_2 , on the plasma properties and CO_2
 492 decomposition. Experiments are carried-out in pure CO_2 and in 96% CO_2 -2% Ar -2% N_2
 493 plasmas, with a gas flow $\Phi = 19.25$ sccm, ignited both in Mars and Earth input gas tem-
 494 peratures. It has been speculated that the presence of traces of Ar and N_2 could be ben-
 495 efiticial for the production of oxygen and carbon monoxide by enhancing CO_2 plasma dis-
 496 sociation (Guerra et al., 2017, 2018), but no experimental evidence has been presented
 497 to date.
 498

499 The measured values of the reduced electric field are shown in Figure 13, the tem-
 500 peratures T_g , T_{12} and T_3 in Figure 14, the temperature ratios T_3/T_g , T_{12}/T_g and T_3/T_{12}
 501 in Figure 15, and the dissociation fraction α in Figure 16. Figures 13-15 indicate that
 502 the presence of Ar and N_2 in the Martian atmosphere has a negligible effect on the re-
 503 duced field and on the vibrational temperatures, maintaining a significant degree of non-
 504 equilibrium. Even though, a small but consistent positive influence on the production
 505 of CO from CO_2 is visible in Figure 16, despite some fluctuation of the results and the
 506 outlier data on Earth at $p \leq 2$ Torr and $I = 50$ mA. It is worth noting that the decom-
 507 position here is lower than what is reported in figure 4. This is due to the lower residence
 508 times of the gas in the plasma, which decrease ~ 3 times as the flow increases.

509 The reasons for a favorable effect of traces of N_2 and Ar in CO_2 decomposition are
 510 most likely due to the modifications induced by Ar and N_2 in the EEDF and by the small

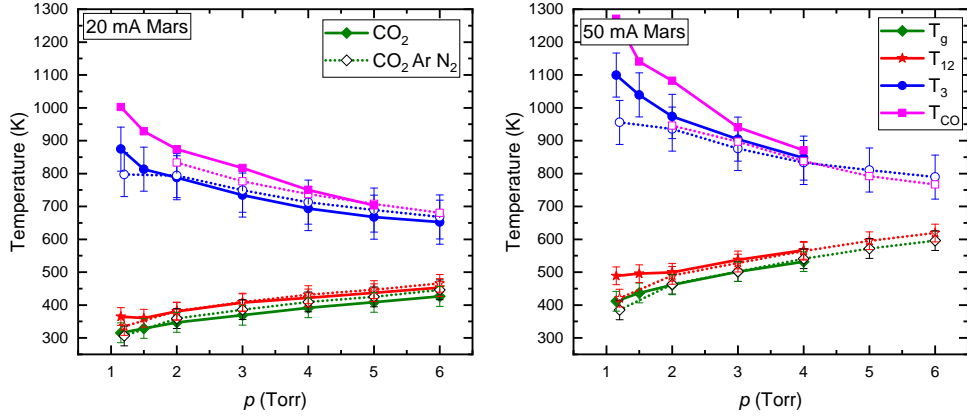


Figure 14. Experimental values of the gas temperature T_g (\blacklozenge, \circ), the vibrational temperature of the asymmetric stretching mode T_3 (\bullet, \circ) and the common vibrational temperature of the bending and symmetric modes T_{12} (\ast, \ast) and CO vibrational temperature T_{CO} (\blacksquare, \square), when pure CO_2 (—, closed symbols) and 96% CO_2 -2%Ar-2% N_2 (\cdots , open symbols) discharges are ignited at Mars background temperature at currents $I = 20$ mA (left panel) and $I = 50$ mA (right panel).

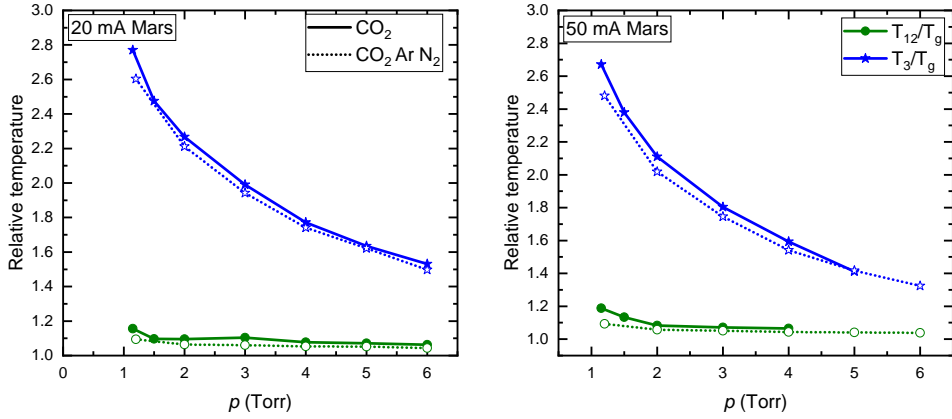


Figure 15. Experimental values of the ratios T_3/T_g (\ast, \ast) and T_{12}/T_g (\bullet, \circ), when pure CO_2 (—, closed symbols) and 96% CO_2 -2%Ar-2% N_2 (\cdots , open symbols) discharges are ignited at Mars background temperature at currents $I = 20$ mA (left panel) and $I = 50$ mA (right panel).

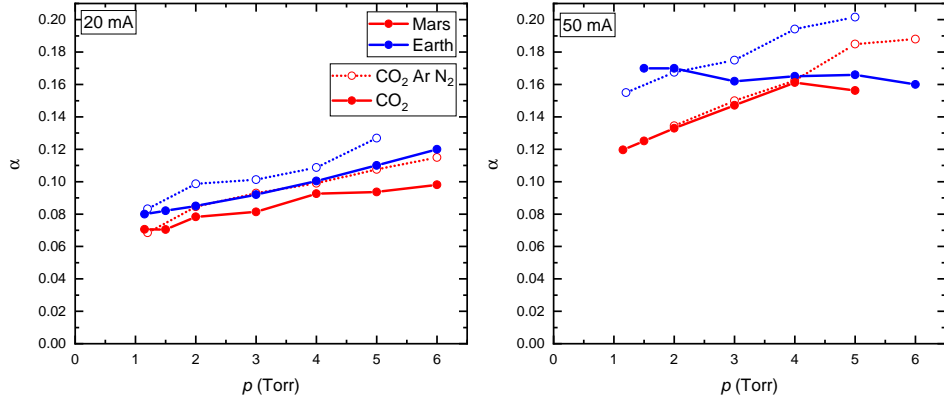


Figure 16. Experimental CO₂ dissociation fraction when pure CO₂ (—●—) and 96%CO₂-2%Ar-2%N₂ (· · ·) discharges are ignited at Mars and Earth background temperatures at currents $I = 20$ mA (left panel) and $I = 50$ mA (right panel)

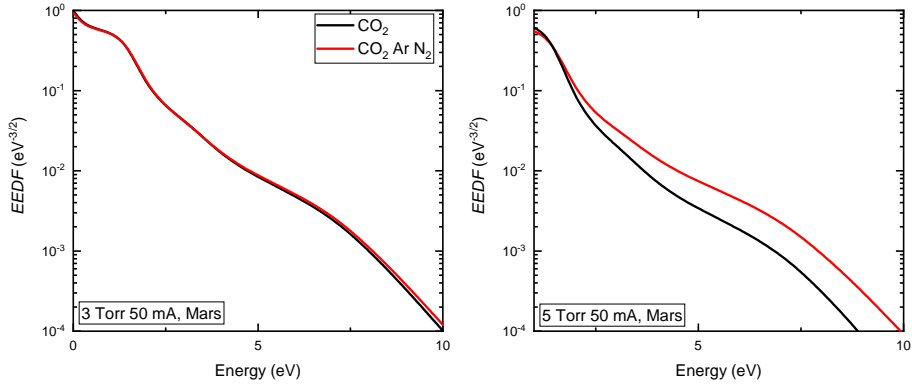


Figure 17. Electron Energy Distribution Functions calculated for the experimental values of E/N , T_{12} , T_3 and T_{CO} at $p = 3$ Torr (left panel) and $p = 5$ Torr (right panel), $I = 50$ mA, and Mars input gas temperature, for pure CO₂ (—) and 96%CO₂-2%Ar-2%N₂ (—).

511 variations in E/N . Figure 17 shows the EEDFs calculated for the experimental condi-
 512 tions of reduced field, E/N , common vibrational temperature of the symmetric stretch-
 513 ing and bending modes, T_{12} , vibrational temperatures of the asymmetric stretching mode,
 514 T_3 , and of CO, T_{CO} , for a discharge ignited at Mars background temperature, current
 515 $I = 50$ mA and pressures $p = 3$ Torr and $p = 5$ Torr, in pure CO₂ and in a synthetic
 516 Martian atmosphere 96%CO₂-2%Ar-2%N₂. The vibrational temperature of N₂ was as-
 517 sumed to be the same as T_{CO} . Figure 17 shows an enhancement of the tail of the EEDF
 518 for the Martian mixture in the region of energies around 7 eV, the energy threshold for
 519 dissociation (Polak & Slovetsky, 1976; Grofulović et al., 2016), which leads to a higher
 520 electron impact dissociation rate coefficient. The effect is specially noticeable for $p = 5$ Torr,
 521 where the observed increase in the dissociation fraction is higher, and is due to the dif-
 522 ferences in the cross sections between the different gases and to a small increase in the
 523 values of E/N when passing from pure CO₂ to CO₂-Ar-N₂ (from 41.9 Td to 42.5 Td at
 524 3 Torr, and from 35.3 Td to 41.1 Td at 5 Torr). Two subtle but identifiable positive ef-
 525 fects are the presence of Ar, that shifts the EEDF to higher energies (Janeco et al., 2015),
 526 and the vibrational temperature of N₂, that enhances the high energy tail via electron
 527 superelastic collisions with vibrationally excited nitrogen.

528 Another possibility for a positive influence of N₂ would be the transfer of vibra-
 529 tional energy from nitrogen to the asymmetric stretching mode of CO₂ and the enhance-
 530 ment of dissociation via the purely vibrational mechanism (Fridman, 2008). Notwith-
 531 standing, the measured vibrational temperatures are not significantly affected and, in
 532 addition, the purely vibrational mechanism does not seem to play a significant role in
 533 the present conditions. Note, however, that the measured vibrational “temperatures”
 534 are only representative of the populations of the lower vibrational levels and do not bring
 535 any information regarding the populations of the higher ones, which may deviate from
 536 equilibrium Boltzmann distributions and be modified by the presence of N₂. A positive
 537 effect of N₂ addition was also observed in experiments by (Grofulović et al., 2019; Ter-
 538 raz et al., 2020), reinforcing the suggestion from Figure 17 that the answer to why the
 539 CO yield is higher in synthetic Martian atmosphere than in pure CO₂ plasmas may lay
 540 in the CO₂-N₂ kinetics. Further research is necessary to elucidate the origin this effect.

541 5 Conclusions

542 This work presents an experimental and modeling investigation on the potential
 543 of low-temperature plasmas for *in situ* resource utilization (ISRU) on Mars. The research
 544 focus on the decomposition of CO₂, which is freely abundant in the Martian atmosphere
 545 and creates the building blocks for the local production of oxygen and fuels.

546 DC glow discharges operating at pressures in the range 0.5-5 Torr are ignited in
 547 pure CO₂ and in a synthetic Martian atmosphere composed of 96%CO₂-2%Ar-2%N₂,
 548 discharge currents $I = 20 - 50$ mA, with the input gas either at Martian (~ 220 K) or
 549 Terrestrial (~ 300 K) temperatures. The CO₂ and CO vibrational temperatures and the
 550 CO and CO₂ concentrations are measured, providing an experimental characterization
 551 of plasmas created in conditions realistically mimicking the atmosphere of Mars.

552 In the system under study, CO₂ is essentially decomposed by direct electron im-
 553 pact, both on molecules in the vibrational ground-state (00⁰0) and in vibrational excited
 554 states. The contribution of the latter states comes mainly from the lower-laying levels (01¹0),
 555 (02²0) and (10⁰0+02⁰0), with several other levels having contributions of a few percent.
 556 Dissociation fractions up to 30% are observed, a very encouraging result considering that
 557 the present setup is designed for fundamental studies and is far from suited for the de-
 558 velopment a prototype.

559 The plasma chemistry is significantly influenced by electronically excited states,
 560 such as O₂($a^1\Delta_g$), O₂($b^1\Sigma_g^+$), O(1D) and CO($a^3\Pi_r$). Therefore, a full control and op-

561 timization of the plasma requires a detailed understanding of the strongly coupled ki-
 562 netics of these states.

563 The results confirm that the Martian conditions of temperature and pressure pump
 564 the asymmetric stretching vibration mode and lead to a stronger degree of non-equilibrium
 565 than on Earth, believed to have a positive influence in dissociation (Fridman, 2008). For
 566 the current discharge configuration, dissociation is driven by electron impact and the con-
 567 version factor at low temperature is slightly lower than at room temperature. Neverthe-
 568 less, vibrational kinetics has a very significant influence in dissociation as a result of elec-
 569 tron superelastic collisions with vibrationally excited CO and CO₂ molecules, that mod-
 570 ify the electron energy distribution function and lead to an increase of the electron im-
 571 pact dissociation rate coefficients and, accordingly, of CO production. Atomic oxygen
 572 is a strong quencher of vibrationally excited CO₂ and has also an important effect in shap-
 573 ing the vibrational distribution functions.

574 The new experimental data corroborate the conjecture of a positive effect of the
 575 Martian atmospheric composition on dissociation advanced in paper (Guerra et al., 2017,
 576 2018). This behavior is most likely related to modifications in the electron kinetics in-
 577 duced by the presence of nitrogen and argon and the associated enhanced dissociation
 578 by electron impact.

579 Despite the beneficial effects of the low ambient temperature and of the presence
 580 of Ar and N₂ in the Martian atmosphere, their impact on CO₂ decomposition is rela-
 581 tively small. Indeed, the results obtained for Mars and Earth background temperatures,
 582 as well as for pure CO₂ and for the synthetic Martian atmosphere, are rather similar in
 583 what concerns the identification of the main creation/destruction mechanisms and all
 584 the trends observed. Thus, knowledge on the energy-transfer pathways acquired on Earth
 585 can, to a very considerable extent, be transposed to Mars.

586 The present results establish experimental evidence of the feasibility of oxygen and
 587 propellant production by plasma decomposition of CO₂ from the Martian atmosphere
 588 and suggest the possible development of more sophisticated setups that can take fully
 589 advantage of non-equilibrium and/or promote dissociation by electron impact. Future
 590 research should concentrate on the design and optimization of robust and efficient plasma
 591 sources and on the procedure to separate O₂ from the other dissociation products. Re-
 592 cent proposals for product separation include the use of silver membranes by Premathilake
 593 et al. (2019) and a new electrochemical membrane reactor presented in (A. P. H. Goede,
 594 2018; Pandiyan et al., 2019).

595 Finally, it is worth noticing that emerging plasma technologies for CO₂ reforming
 596 on Earth are already expected to be competitive with solid oxide electrolysis (SOEC)
 597 (van Rooij et al., 2015; den Harder et al., 2017; Boagerts & Neyts, 2018), the technol-
 598 ogy proposed in NASA’s MOXIE program. Therefore, a plasma-electrochemical process
 599 will most certainly be a viable alternative to SOEC for oxygen production on Mars. In
 600 fact, the efficiency of SOEC is likely to decrease as compared to that on Earth, because
 601 extra energy is necessary to compress the gas up to 1 atm, pre-heat it up to 1100 K and
 602 cool down the exhaust stream (Hecht et al., 2014; Hecht & Hoffman, 2016). Furthermore,
 603 sophisticated thermal insulation systems are mandatory. In turn, the efficiency of plasma
 604 dissociation of CO₂ on Mars is likely to increase as compared to that on Earth, due to
 605 the beneficial effects demonstrated in this paper and the absence of vacuum pumps. A
 606 conservative estimation can be made as follows. Consider a thermodynamic value of ~
 607 50% energy efficiency for gas phase dissociation, as reached recently by den Harder et
 608 al. (2017), marginally amplified by the interaction with catalytic walls and membrane
 609 to about 55%. At 300 W it corresponds to the production of 35g of O₂ per hour, at an
 610 energy cost of 10 eV/molecule. A decrease in performance of about 50%, to account for
 611 unexpected difficulties and the uncertainties of development of a new technology, brings
 612 these numbers to approximately 20 g of O₂ per hour, at an energy cost of 18 eV per molecule

613 and 31% energy efficiency. These rather prudent values outperform the most optimistic
 614 predictions of MOXIE by 100% and bring further evidence in favor of the plausibility
 615 and significance of plasma ISRU on Mars as a complementary technology to SOEC.

616 Author contributions

617 Conceptualization: VG; Methodology: ASMC, OG, PO, VG; Software: AFS, ATC, LLA,
 618 PO, TS; Validation: ASMC, PO; Formal Analysis: ASMC, PO; Investigation: ASMC,
 619 PO; Resources: OG; Writing - original draft: PO, VG; Writing - review and editing: ASMC,
 620 ATC, LLA, OG, TS, VG; Visualization: PO; Supervision: OG, VG; Project adminis-
 621 tration: OG, VG; Funding acquisition: LLA, OG, VG.

622 Acknowledgments

623 This work was partially funded by Portuguese FCT - Fundação para a Ciência e a Tec-
 624 nologia, under projects UIDB/50010/2020 and UIDP/50010/2020 and grant PD/BD/114398/2016
 625 (PD-F APPLAuSE).

626 Upon acceptance of the paper, all data will be made available from the repository of the
 627 Instituto de Plasmas e Fusão Nuclear, Instituto Superior Técnico.

628 References

- 629 Alves, L. L., Coche, P., Ridenti, M. A., & Guerra, V. (2016). Electron scattering
 630 cross sections for the modelling of oxygen-containing plasmas. *Eur. Phys. J.*
 631 *D*, *70*, 124. doi: 10.1140/epjd/e2016-70102-1
- 632 Annaloro, J., & Bultel, A. (2019). Vibrational and electronic collisional-radiative
 633 model in CO₂-N₂-Ar mixtures for mars entry problems. *Phys. Plasmas*, *26*,
 634 103505. doi: 10.1063/1.5114792
- 635 Annušová, A., Marinov, D., Booth, J. P., Sirse, N., Lino da Silva, M., Lopez, B., &
 636 Guerra, V. (2018). Kinetics of highly vibrationally excited O₂(X) molecules in
 637 inductively-coupled oxygen plasmas. *Plasma Sources Sci. Technol.*, *27*, 045006.
 638 doi: 10.1088/1361-6595/aab47d
- 639 Ash, R. L., Dowler, W. L., & Varsi, G. (1978). Feasibility of rocket propellant pro-
 640 duction on mars. *Acta Astronaut.*, *5*, 705-724. doi: 10.1016/0094-5765(78)
 641 90049-8
- 642 Ash, R. L., Wu, D., & Outlaw, R. A. (1994). A study of glow-discharge and perme-
 643 ation techniques for extraterrestrial oxygen beneficiation. *Adv. Space Res.*, *14*,
 644 (6)259–(6)263.
- 645 Boagerts, A., & Neyts, E. C. (2018). Plasma technology: An emerging technology-
 646 for energy storage. *ACS Energy Lett.*, *3*, 1013-1027. doi: 10.1021/acsenerylett
 647 .8b00184
- 648 Boiron, A. J., & Cantwell, B. J. (2013). Hybrid rocket propulsion and in-situ pro-
 649 pellant production for future mars missions. In *49th aiaa/asme/sae/asee joint*
 650 *propulsionconference* (p. 3899). San Jose, CA. doi: 10.2514/6.2013-3899
- 651 Catalfamo, C., Bruno, D., Colonna, G., Laricchiuta, A., & Capitelli, M. (2009). High
 652 temperature Mars atmosphere. Part II: transport properties. *Eur. Phys. J. D*,
 653 *54*, 613-621. doi: 10.1140/epjd/e2009-00193-6
- 654 Celiberto, R., Armenise, I., Cacciatore, M., Capitelli, M., Esposito, F., Gamallo, P.,
 655 ... Wadehra, J. M. (2016). Atomic and molecular data for spacecraft re-entry
 656 plasmas. *Plasma Sources Sci. Technol.*, *25*, 033004.
- 657 Celiberto, R., Laporta, V., Laricchiuta, A., Tennyson, J., & Wadehra, J. M. (2014).
 658 Molecular physics of elementary processes relevant to hypersonics: Electron-
 659 molecule collisions. *Open Plasma Phys. J.*, *7 (suppl 1:M2)*, 33–47.
- 660 Cosby, P. C. (1993). Electron-impact dissociation of carbon monoxide. *J. Chem.*

- 661 *Phys.*, 98(10), 7804–7818. Retrieved from [https://doi.org/10.1063/](https://doi.org/10.1063/1.464588)
662 1.464588 doi: 10.1063/1.464588
- 663 den Harder, N., van den Bekerom, D. C. M., Al, R. S., Graswinckel, M. F., Palo-
664 mares, J. M., Peeters, F. J. J., ... van Rooij, G. J. (2017). Homogeneous CO₂
665 conversion by microwave plasma: Wave propagation and diagnostics. *Plasma*
666 *Process. Polym.*, 14, e1600120. doi: 10.1039/c5fd00045a
- 667 Fridman, A. (2008). *Plasma Chemistry*. Cambridge University Press. doi: 10.1017/
668 CBO9780511546075
- 669 Goede, A., & van de Sanden, R. (2017). CO₂ neutral fuels. *EPN*, 47/3, 22-25. doi:
670 10.1051/epn/2016304
- 671 Goede, A. P. H. (2018). CO₂ neutral fuels. *EPJ Web Conf.*, 189, 00010. doi: 10
672 .1051/epjconf/201818900010
- 673 Grofulović, M., Alves, L. L., & Guerra, V. (2016). Electron-neutral scattering cross
674 sections for CO₂: a complete and consistent set and an assessment of dissoci-
675 ation. *J. Phys. D: Appl. Phys.*, 49, 395207. doi: 10.1088/0022-3727/49/39/
676 395207
- 677 Grofulović, M., Klarenaar, B. L. M., Guaitella, O., Guerra, V., & Engeln, R. (2019).
678 A rotational Raman study under non-thermal conditions in pulsed CO₂-N₂
679 and CO₂-O₂ glow discharges. *Plasma Sources Sci. Technol.*, 28, 045014. doi:
680 10.1088/1361-6595/ab1240
- 681 Grofulović, M., Silva, T., Klarenaar, B. L. M., Morillo-Candas, A. S., Guaitella, O.,
682 Engeln, R., ... Guerra, V. (2018). Kinetic study of CO₂ plasmas under non-
683 equilibrium conditions. II. Input of vibrational energy. *Plasma Sources Sci.*
684 *Technol.*, 27, 015009. doi: 10.1088/1361-6595/aadb60
- 685 Gruenewald, J. (2014). A proposal for a plasma technology based hybrid life sup-
686 port system for future Mars habitats. *J. Space Technol.*, 4, 1–6.
- 687 Guerra, V., & Loureiro, J. (1997). Electron and heavy particle kinetics in a low pres-
688 sure nitrogen glow discharge. *Plasma Sources Sci. Technol.*, 6, 361–372.
- 689 Guerra, V., & Loureiro, J. (1999). Kinetic model of a low pressure microwave
690 discharge in O₂-N₂ including the effects of O⁻ ions on the characteristics for
691 plasma maintenance. *Plasma Sources Sci. Technol.*, 6, 373–385.
- 692 Guerra, V., Silva, T., & Guaitella, O. (2018). Living on Mars: how to produce oxy-
693 gen and fuel to get home. *EPN*, 49/2, 15-18.
- 694 Guerra, V., Silva, T., Ogloblina, P., Grofulović, M., Terraz, L., Lino da Silva, M., ...
695 Guaitella, O. (2017). The case for in situ resource utilisation for oxygen pro-
696 duction on Mars by non- equilibrium plasmas. *Plasma Sources Sci. Technol.*,
697 26, 11LT01.
- 698 Guerra, V., Tatarova, E., Dias, F. M., & Ferreira, C. M. (2002). On the self-
699 consistent modeling of a traveling wave sustained nitrogen discharge. *J. Appl.*
700 *Phys.*, 91, 2648–2661.
- 701 Haberle, R. M. (2015). Solar System/Sun, Atmospheres, Evolution of Atmospheres.
702 Planetary Atmospheres: Mars. In *Encyclopedia of atmospheric sciences* (2nd
703 ed., Vol. 5, pp. 168–177). Elsevier. doi: 10.1016/B978-0-12-382225-3.00312-1
- 704 Hartvigsen, J. J., Elangovan, S., Larsen, D., Elwell, J., Bokil, M., Frost, L., & Clark,
705 L. M. (2015). Challenges of solid oxide electrolysis for production of fuel and
706 oxygen from mars atmospheric CO₂. *ECS Transactions*, 68, 3563-3583.
- 707 Hecht, M. H., & Hoffman, J. A. (2016). The mars oxygen ISRU experiment
708 (MOXIE) on the mars 2020 rover. In *3rd international workshop on instru-*
709 *mentation for planetary missions* (p. 4130). Pasadena, CA.
- 710 Hecht, M. H., Rapp, D. R., & Hoffman, J. A. (2014). The Mars Oxygen ISRU ex-
711 periment (MOXIE). In *International workshop on instrumentation for plane-*
712 *tary missions* (p. 1134). Greenbelt, MD.
- 713 IEA. (2019). *Global energy & CO₂ status report 2019*. International Energy Agency,
714 <https://www.iea.org/reports/global-energy-co2-status-report-2019>.

- 715 Itikawa, Y. (2015). Cross sections for electron collisions with carbon monoxide. *J.*
716 *Phys. Chem. Ref. Data*, *44*, 013105. doi: 10.1063/1.4913926
- 717 Janeco, A., Pinhão, N. R., & Guerra, V. (2015). Electron kinetics in He/CH₄/CO₂
718 mixtures used for methane conversion. *J. Phys. Chem. C*, *119*, 109-120.
- 719 Klarenaar, B. L. M., Engeln, R., van den Bekerom, D. C. M., van de Sanden,
720 M. C. M., Morillo-Candas, A. S., & Guaitella, O. (2017). Time evolution
721 of vibrational temperatures in a CO₂ glow discharge measured with infrared
722 absorption spectroscopy. *Plasma Sources Sci. Technol.*, *26*, 115008.
- 723 Klarenaar, B. L. M., Morillo-Candas, A. S., Grofulović, M., van de Sanden,
724 M. C. M., Engeln, R., & Guaitella, O. (2019). Excitation and relaxation
725 of the asymmetric stretch mode of CO₂ in a pulsed glowdischarge. *Plasma*
726 *Sources Sci. Technol.*, *28*, 035011. doi: 10.1088/1361-6595/aada5e
- 727 Laher, R. R., & Gilmore, F. R. (1990). Updated excitation and ionization cross
728 sections for electron impact on atomic oxygen. *J. Phys. Chem. Ref. Data*, *19*,
729 277. doi: 10.1063/1.555872
- 730 Landis, G. A., & Linne, D. L. (2001). Mars Rocket Vehicle Using In Situ Propel-
731 lants. *Journal of Spacecraft and Rockets*, *38*(5), 730-735. doi: 10.2514/2.3739
- 732 Laporta, V., Cassidy, C. M., Tennyson, J., & Celiberto, R. (2012). Electron-
733 impact resonant vibration excitation cross sections and rate coefficients
734 for carbon monoxi. *Plasma Sources Sci. Technol.*, *21*, 045005. doi:
735 10.1088/0963-0252/21/4/045005
- 736 Laricchiuta, A., Bruno, D., Capitelli, M., Catalfamo, C., Celiberto, R., Colonna,
737 G., ... Pirani, F. (2009). High temperature Mars atmosphere. Part I:
738 transport cross sections. *Eur. Phys. J. D*, *54*, 607-612. doi: 10.1140/epjd/
739 e2009-00192-7
- 740 Lawton, S. A., & Phelps, A. V. (1978). Excitation of the $b^1\Sigma_g^+$ state of O₂ by low
741 energy electrons. *J. Chem. Phys.*, *69*, 1055. doi: 10.1063/1.436700
- 742 *The LisbOn KInetics - LoKI*. (2019). Retrieved 2020, from [https://nprime](https://nprime.tecnico.ulisboa.pt/loki/tools.html)
743 [.tecnico.ulisboa.pt/loki/tools.html](https://nprime.tecnico.ulisboa.pt/loki/tools.html);[https://github.com/IST-Lisbon/](https://github.com/IST-Lisbon/LoKI)
744 [LoKI](https://github.com/IST-Lisbon/LoKI)
- 745 Lowke, J. ., Phelps, A. V., & Irwin, B. W. (1973). Predicted electron transport co-
746 efficients and operating characteristics of CO₂-N₂-He laser mixtures. *J. Appl.*
747 *Phys.*, *44*, 4664.
- 748 Manning, H. L. K., ten Kate, I. L., Battel, S. J., & Mahaff, P. R. (2010).
749 Electric discharge in the martian atmosphere, Paschen curves and im-
750 plications for future missions. *Adv. Space Res.*, *46*, 13340-1340. doi:
751 10.1016/j.asr.2010.07.006
- 752 Garcia-Cosio, G., Martinez, H., Calixto-Rodriguez, M., & Gomez, A. (2011). DC
753 discharge experiment in an Ar/N₂/CO₂ ternary mixture: A laboratory simula-
754 tion of the martian ionosphere's plasma environment. *JQSRT*, *112*, 2787-2793.
755 doi: 10.1016/j.jqsrt.2011.09.008
- 756 López-Puertas, M., Rodrigo, R., López-Moreno, J. J., & Taylor, F. W. (1986). A
757 non-LTE radiative transfer model for infrared bands in the middle atmosphere.
758 II. CO₂ (2.7 and 4.3 μm) and water vapour (6.3 μm) bands and N₂(1) and
759 O₂(1) vibrational levels. *J. Atmospheric Terr. Phys.*, *48*, 749-746.
- 760 Morillo-Candas, A. S. (2019). *Investigation of fundamental mechanisms of CO₂ plas-*
761 *mas* (PhD thesis). Ecole Polytechnique - Université Paris-Saclay.
- 762 Morillo-Candas, A. S., Drag, C., Booth, J. P., Dias, T. C., Guerra, V., & Guaitella,
763 O. (2019). Oxygen atom kinetics in CO₂ plasmas ignited in a DC glow dis-
764 charge. *Plasma Sources Sci. Technol.*, *28*, 075010. doi: 10.1088/1361-6595/
765 ab2b84
- 766 Morillo-Candas, A. S., Guerra, V., & Guaitella, O. (2020). Time evolution of the
767 dissociation fraction in RF CO₂ plasmas: impact and nature of back reaction
768 mechanisms. *Plasma Sources Sci. Technol.*. doi: 10.1021/acs.jpcc.0c03354

- 769 Morillo-Candas, A. S., Klarenaar, B. L. M., Amoedo, C., Guerra, V., & Guaitella,
770 O. (2020). Effect of oxygen atoms on the vibrational kinetics of CO₂ and CO
771 revealed by the use of a large surface area material. *J. Phys. D: Appl. Phys.*
772 doi: 10.1088/1361-6463/abc992
- 773 Morillo-Candas, A. S., Silva, T., Klarenaar, B. L. M., Grofulović, M., Guerra, V., &
774 Guaitella, O. (2020). Electron impact dissociation of CO₂. *Plasma Sources*
775 *Sci. Technol.*, 29, 01LT01. doi: 10.1088/1361-6595/ab2b84
- 776 NASA. (2020). *Chronology of Mars Exploration*. Retrieved from [https://nssdc](https://nssdc.gsfc.nasa.gov/planetary/chronology_mars.html)
777 [.gsfc.nasa.gov/planetary/chronology_mars.html](https://nssdc.gsfc.nasa.gov/planetary/chronology_mars.html)
- 778 Ogloblina, P., Guerra, V., Morillo-Candas, A. S., & Guaitella, O. (2019). Plasma
779 reforming for oxygen production on mars. In *8th european conference for aero-*
780 *navitics and aero-space sciences (EUCASS)*.
- 781 Ogloblina, P., Tejero-del-Caz, A., Guerra, V., & Alves, L. L. (2020). Electron im-
782 pact cross sections for carbon monoxide and their importance in the electron
783 kinetics of CO₂–CO mixtures. *Plasma Sources Sci. Technol.*, 29, 015002. doi:
784 10.1088/1361-6595/ab4e72
- 785 Outlaw, R. A. (1990). O₂ and CO₂ glow-discharge-assisted oxygen transport
786 through Ag. *J. Appl. Phys.*, 68, 1002–1004.
- 787 Pack, R. T. (1980). Analytic estimation of almost resonant molecular energy transfer
788 due to multipolar potentials. VV processes involving CO₂. *J. Chem. Phys.*, 72,
789 6140–6152.
- 790 Pandiyan, A., Neagu, D., Kyriakou, V., Sharma, R., Middelkoop, V., Weber, S., ...
791 Tsampas, M. (2019). Electrochemical membrane reactor for oxygen separa-
792 tion after CO₂ plasmolysis. In *14th international conference on catalysis in*
793 *membrane reactors (iccmr-14)*.
- 794 Phelps, A. V. (1985). *Tabulations of collision cross sections and calculated transport*
795 *and reaction coefficients for electron collisions with O₂* (Tech. Rep. No. 28).
796 JILA Information Center Report. (University of Colorado, Boulder, Colorado,
797 USA)
- 798 Pietanza, L. D., Colonna, G., & Capitelli, M. (2020). Self-consistent electron energy
799 distribution functions, vibrational distributions, electronic excited state kinet-
800 ics in reacting microwave CO₂ plasma: An advanced model. *Phys. Plasmas*,
801 27, 023513. doi: 10.1063/1.5139625
- 802 *Plasma data exchange project*. (2010). Retrieved 2020, from www.lxcat.net
- 803 Polak, L. S., & Slovetsky, D. I. (1976). Electron impact induced electronic excita-
804 tion and molecular dissociation. *Int. J. Radiat. Phys. Chem.*, 8, 257-282. doi:
805 10.1016/0020-7055(76)90070-X
- 806 Premathilake, D., Outlaw, R. A., Quinlan, R. A., & Byvik, C. E. (2019). Oxy-
807 gen generation by carbon dioxide glow discharge and separation by perme-
808 ation through ultrathin silver membranes. *Earth and Space Science*. doi:
809 10.1029/2018EA000521
- 810 Raizer, Y. P. (1991). *Gas discharge physics* (J. E. Allen, Ed.). Springer-Verlag.
- 811 Rapp, D., & Briglia, D. D. (1965). Total cross sections for ionization and attach-
812 ment in gases by electron impact. II. Negative-ion formation. *J. Chem. Phys.*,
813 43(5), 1480–1489. Retrieved from [http://aip.scitation.org/doi/10.1063/](http://aip.scitation.org/doi/10.1063/1.1696957)
814 [1.1696957](http://aip.scitation.org/doi/10.1063/1.1696957) doi: 10.1063/1.1696957
- 815 Rapp, D., & Englander-Golden, P. (1965). Total cross sections for ionization and
816 attachment in gases by electron impact. I. Positive ionization. *J. Chem. Phys.*,
817 43, 1464–1479.
- 818 Sanders, G. B., Paz, A., Oryshchyn, L., & Araghi, K. (2015). Mars ISRU for Pro-
819 duction of Mission Critical Consumables – Options , Recent Studies , and
820 Current State of the Art. *SPACE Conferences and Exposition*, 1–14. doi:
821 doi:10.2514/6.2015-4458
- 822 Sawada, T., Sellin, D. L., & Green, A. E. S. (1972). Electron impact excitation
823 cross sections and energy degradation in CO. *J. Geophys. Res.*, 77(25), 4819–

- 824 28. doi: 10.1029/JA077i025p04819
- 825 Shofield, K. (1979). Critically evaluated rate constants for gaseous reactions of sev-
- 826 eral electronically excited species. *J. Phys. Chem. Ref. Data*, *8*, 723-798. doi:
- 827 10.1063/1.555606
- 828 Silva, A. F., Morillo-Candas, A. S., Tejero-del-Caz, A., Alves, L. L., Guaitella, O., &
- 829 Guerra, V. (2020). A reaction mechanism for vibrationally cold CO₂ plasmas.
- 830 *Plasma Sources Sci. Technol.* doi: 10.1088/1361-6595/abc818
- 831 Silva, T., Grofulović, M., Klarenaar, B. L. M., Guaitella, O., Engeln, R., Pintas-
- 832 silgo, C. D., & Guerra, V. (2018). Kinetic study of CO₂ plasmas under
- 833 non-equilibrium conditions. I. Relaxation of vibrational energy. *Plasma Sources*
- 834 *Sci. Technol.*, *27*, 015019. doi: 10.1088/1361-6595/aaa56a
- 835 Silva, T., Grofulović, M., Terraz, L., Pintassilgo, C. D., & Guerra, V. (2018). Mod-
- 836 elling the input and relaxation of vibrational energy in CO₂ plasmas. *J. Phys.*
- 837 *D: Appl. Phys.*, *51*, 464001. doi: 10.1088/1361-6463/aadbd7
- 838 Silva, T., Grofulović, M., Terraz, L., Pintassilgo, C. D., & Guerra, V. (2020).
- 839 Dynamics of gas heating in the afterglow of pulsed CO₂ and CO₂-N₂
- 840 glow discharges at low pressure. *Plasma Chem. Plasma Process.* doi:
- 841 10.1007/s11090-020-10061-7
- 842 Stancati, M. L., Niehoff, J. C., Wells, W. C., & Ash, R. L. (1979). Hybrid rocket
- 843 propulsion and in-situ propellant production for future mars missions. In *Con-*
- 844 *ference on advanced technology for future space systems* (p. 906). Hampton,
- 845 VA. doi: 10.2514/6.1979-906
- 846 Tejero-del-Caz, A., Alves, L. L., Guerra, V., Gonçalves, D., Lino da Silva, M.,
- 847 Pinhão, N., ... Pintassilgo, C. D. (2018). The LisbOn KInetics tool suit.
- 848 In *71st annual gaseous electronics conference* (p. GT1.071). Portland, OR. doi:
- 849 10.1088/1361-6595/ab0537
- 850 Tejero-del-Caz, A., Guerra, V., Gonçalves, D., Lino da Silva, M., Marques, L.,
- 851 Pinhão, N., ... Alves, L. L. (2019). The LisbOn KInetics Boltzmann solver.
- 852 *Plasma Sources Sci. Technol.*, *28*, 043001. doi: 10.1088/1361-6595/ab0537
- 853 Terraz, L., Silva, T., Morillo-Candas, A., Guaitella, O., Tejero-del-Caz, A., Alves,
- 854 L. L., & Guerra, V. (2020). Influence of N₂ on the CO₂ vibrational distribu-
- 855 tion function and dissociation yield in non-equilibrium plasmas. *J. Phys. D:*
- 856 *Appl. Phys.*, *53*, 094002. doi: 10.1088/1361-6463/ab55fb
- 857 van Rooij, G. J., van den Bekerom, D. C. M., den Harder, N., Minea, T., Berden,
- 858 G., Bongers, W. A., ... van de Sanden, M. C. M. (2015). Taming mi-
- 859 crowave plasma to beat thermodynamics in CO₂ dissociation. *Faraday dis-*
- 860 *ussions*, *183*, 233-248. Retrieved from [http://pubs.rsc.org/en/Content/](http://pubs.rsc.org/en/Content/ArticleHTML/2015/FD/C5FD00045A)
- 861 [ArticleHTML/2015/FD/C5FD00045A](http://pubs.rsc.org/en/Content/ArticleHTML/2015/FD/C5FD00045A) doi: 10.1039/c5fd00045a
- 862 Wu, D., Outlaw, R. A., & Ash, R. L. (1996). Extraction of oxygen from CO₂ using
- 863 glow-discharge and permeation techniques. *J. Vac. Sci. Technol. A*, *14*, 408-
- 864 414.